

Review

A review of piezoelectric MEMS sensors and actuators for gas detection application

Saeed S. Ba Hashwan¹ · Mohd Haris Md. Khir¹ · Illani Mohd Naw¹ · Mohamad Radzi Ahmad¹ · Mehwish Hanif¹ · Furqan Zahoor¹ · Y. Al-Douri^{2,3,4} · Abdullah Saleh Algamili¹ · Usman Isyaku Bature¹ · Sami Sultan Alabsi¹ · Mohammed O. Ba Sabbea⁵ · Muhammad Junaid^{1,6}

Received: 17 November 2022 / Accepted: 25 January 2023

© The Author(s) 2023, corrected publication 2023 **OPEN**

Published online: 27 February 2023

Abstract

Piezoelectric microelectromechanical system (piezo-MEMS)-based mass sensors including the piezoelectric microcantilevers, surface acoustic waves (SAW), quartz crystal microbalance (QCM), piezoelectric micromachined ultrasonic transducer (PMUT), and film bulk acoustic wave resonators (FBAR) are highlighted as suitable candidates for highly sensitive gas detection application. This paper presents the piezo-MEMS gas sensors' characteristics such as their miniaturized structure, the capability of integration with readout circuit, and fabrication feasibility using multiuser technologies. The development of the piezoelectric MEMS gas sensors is investigated for the application of low-level concentration gas molecules detection. In this work, the various types of gas sensors based on piezoelectricity are investigated extensively including their operating principle, besides their material parameters as well as the critical design parameters, the device structures, and their sensing materials including the polymers, carbon, metal–organic framework, and graphene.

Keywords Microelectromechanical system (MEMS) · Gas sensors · Piezoelectric actuators · Sensing principle · Microcantilever · QCM · SAW · BAW · PMUT · FBAR · Sensing layers

Abbreviations

MEMS	Microelectromechanical system
Piezo-MEMS	Piezoelectric microelectromechanical system
QCM	Quartz crystal microbalance
SAW	Surface acoustic waves
PMUT	Piezoelectric micromachined ultrasonic transducer

✉ Saeed S. Ba Hashwan, saeedsb2013@gmail.com | ¹Department of Electrical and Electronic Engineering, Universiti Teknologi PETRONAS, 32610 Seri Iskandar, Malaysia. ²Nanotechnology and Catalysis Research Centre (NANOCAT), University of Malaya, Kuala Lumpur, Malaysia. ³Department of Mechanical Engineering, Faculty of Engineering, Piri Reis University, Eflatun Sk. No: 8, 34940 Tuzla, Istanbul, Turkey. ⁴Department of Applied Science and Astronomy, College of Sciences, University of Sharjah, Sharjah, United Arab Emirates. ⁵Department of Electrical and Computer Engineering, University of Waterloo, Waterloo, ON N2L 3G1, Canada. ⁶Department of Electronic Engineering, Balochistan University of Information Technology, Engineering and Management Sciences, Quetta 87300, Pakistan.



Discover Nano (2023) 18:25 | <https://doi.org/10.1186/s11671-023-03779-8>

FBAR	Film bulk acoustic wave resonators
FPAR	Film plate acoustic resonators
LE	Lateral extensional mode
LFE	Lateral field excitation
Flex	Flexural mode
TE	Thickness extensional mode
CMR	Contour-mode resonator
TSM	Thickness shear mode
APW	Acoustic plate wave
BAW	Bulk acoustic wave
SH-SAW	Shear horizontal acoustic wave
AlN	Aluminum nitride

Introduction

Microelectromechanical systems (MEMS) originally referred to the integration of the mechanical and electrical components at the microscale and nanoscale dimensions. The main purpose and function of the MEMS are to collect physical and chemical information such as pressure, temperature, chemical and gases molecules from the surrounding environment and deliver this information in a more suitable form to human senses [1]. Undoubtedly, the task of gathering and transforming information is usually performed by sophisticated technical systems. However, MEMS devices are capable to perform these tasks despite their small sizes [2]. In addition, MEMS can be defined as miniaturized mechanical and electromechanical elements that are made through microfabrication techniques with dimensions varying from below one micron in the smallest elements all the way to several millimeters [2–7]. MEMS devices have been designed in several structural varying from simple structural with an element that does not perform any movement to extremely complex electromechanical system that contained multiple elements that performed sophisticated action and movement under the control of integrated microelectronic circuits [8].

The well-addressed components of the MEMS devices are the microsensors and microactuators, also known as “transducers,” which are defined as the elements that perform the task of converting the energy or power from one domain to other domains [9]. For instance, the sensors can convert a measured physical signal into an electrical signal, whereas the actuators can convert the electrical signals into mechanical signals just to move themselves or any other components from one position into another state inside the system. In particular, the sensors are the devices that detect and monitor events or changes in the environment such as gas, chemical, pressure, temperature, vibration, and flow. On the other hand, the actuator transducer is the part of the system that helps to achieve physical/mechanical movement after receiving energy in the form of electrical or other forms of energy. There are various actuators such as pneumatic actuators [10] where their input is air, as well as piezoelectric actuators [11] where their inputs are current or voltage, the micro-valves for controlling the gas and liquid flows, as well as the micro-pumps for fluids pressures [12] that have been used in medical devices and many more. In fact, the output in the actuators is always in the mechanical form of energy [13]. In simple words, the sensing process can be defined as energy transduction that provides us with understanding signals or recognition of unknown actions, whereas the actuation process can be classified as the energy conversion that produces mechanical actions [14, 15].

In addition, MEMS is one of the most promising technologies of the twenty-first century; it has the potential to significantly alter all aspects of our lives and the way we live in the future [16]. MEMS along with the combination of silicon-based microelectronics and micromachining technology has dramatically revolutionized both the industry technologies and consumer products from high-technology machines to tiny elements in smartphones. Scientists believe that the MEMS revolution is going to be the second revolution in micromanufacturing after the semiconductor microfabrication revolution.

The arguable history of MEMS began back on April 1, 1954, when C.S smith [17] from Bell Telephone Lab published in a physical review journal describing the basics of MEMS for the first time which related to the certain stress–strain effects in the silicon and germanium called the piezoresistance. Since then, the researchers have extensively investigated the technologies that have made the transistor and its feasibility to produce sensors and trying to produce electrochemical systems with smaller dimensions [1, 18]. In 1959, a famous talk has been conducted by Richard Feynman entitled “There

is plenty of room at the bottom” and he published a summary of the talk later in 1992 [19]. He was interested in exploring how to produce complex motors and machines with multi-functions on a small scale [20]. Richard Feynman and Gordon Moore are only examples of the early scientists who predicted the emerging technologies that could produce tiny microsystems. Currently, new MEMS technologies and applications are being developed every single day globally. Additionally, MEMS are being manufactured using a variety of materials such as semiconductors, biomaterials, nanomaterials, magnetic, piezoelectric, ferroelectric, ceramic, and plastics [11, 21–24]. In addition, MEMS devices can be used in various applications such as sensors, actuators, switches, inertial sensors including (gyroscopes and accelerometers), optical scanners, miniature robots, micro-mirrors, and many more applications are being developed every day [25–33].

In the last few years, MEMS fabrication technology has grown dramatically to the point that tiny devices can be manufactured to be working as actuators and sensors; therefore, they can be found everywhere from wearable devices to automotive equipment [29, 30, 34]. The fabrication techniques used in MEMS production combine the capabilities of the techniques that are utilized in the IC domain with the processes of micromachining such as surface micromachining, bulk micromachining, Lithographie Galvanoformung Abformung (LIGA), high-aspect-ratio micromachining (HARM) to wafer bonding and molding, etc. [30]. MEMS CAP Inc., USA, is one of the famous companies that provides MEMS fabrication facilities for researchers through multiusers MEMS procedures (MUMPs) including several standard fabrication procedures such as MetalMUMPs [35], PolyMUMPs [36], SOIMUMP [37], and PiezoMUMPs [38], whereas there are hundreds of other fabs in the global who are fabricating MEMS devices, just to mention some, including SiTerra [39–41], Infineon [42], CEA-LETI [43, 44], CSEM [45], TSMS [46, 47], and Bosh [48, 49].

Over the above, MEMS technology has been utilized widely in the development of gas and chemical sensors [28]. Moreover, MEMS devices have been used for gas detection including sulfur dioxide (SO₂) [50], carbon dioxide (CO₂) [51], nitrogen dioxide (NO₂) [52], and a few more gases that are constantly released by industry into the environment in the industrialization era. There are various gas sensors utilized in MEMS technologies including capacitive sensing [53], piezoresistive sensing [54, 55], optical sensing [56], and piezoelectric sensing methods [15]. In this review paper, the piezoelectric sensing methods for gas detection applications are presented in detail. There has been significant improvement in the piezoelectric acoustic resonators for gases detection routes such as microcantilever [57, 58], surface acoustic wave (SAW) [59], quartz crystal microbalance (QCM) [60], film bulk acoustic resonator (FBAR) [61], and piezoelectric micromachined ultrasound transducers (PMUT) [62].

Furthermore, nanomaterials that have been used as sensing layers in the gas sensors are playing important roles in the sensor's structures and functions. The development of sensitive nanomaterials has grown dramatically to enhance and optimize the performance and compatibility of MEMS-based gas sensors. There are various nanomaterials have been developed for sensing toxic and harmful gases. Some of the existing materials are including metal oxide semiconductors (MOS) [63], nanometals particles [64, 65], transition metal dichalcogenides (TMDs) [66], carbon nanotubes and their derivatives [23], graphene and its derivatives [23, 67], and metal–organic frameworks (MOFs) [68], etc., which possess remarkable properties such as high surface to volume ratio, high sensitivity, good reversibility, chemical stability, special chemical bonds, and excellent electrical properties. The combination of highly sensitive nanomaterials and highly precise microfabrication technologies brings a novel solution for gas sensor development. In addition, researchers and scientists have extensively investigated several strategies for enhancing the performance of the gases sensors such as optimizing the device geometry [69], optimizing novel fabrication processes [70], enhancing the resonant frequency as in mass-sensitive sensors [71], and exploring new novel ultrasensitive materials [72, 73]. However, the metal oxide semiconductor sensors are working based on high temperature [74], which not only increase the power consumption but also cause some material defects and safety issues. Therefore, the gas sensors to some extent are vigorously dependent on the novel characteristics of the nanomaterials [75, 76]. In more detail, there are abundant types of nanomaterials that have been developed in various structures and used in the gas sensors such as 0D nanoparticles [77], 0D quantum dots [78], 1D nanowires [79], 1D nanofibers [80], 1D carbon nanotubes [81], 1D nanorods [82], 2D nanosheets [83], 2D honeycomb-like [84] and 3D hierarchical microsphere architectures [85, 86].

Zhu et al. [87] have summarized the future trends of the MEMS device and their application from the 1950s to the current devices. They have summarized various important aspects in the MEMS industries, including the critical microfabrication processes technologies, their operation frequencies, reduction in power consumption, and signal noise. In addition, the future MEMS trends have been addressed such as the wearable MEMS and the adaption of machine learning technologies which help to overcome certain issues in MEMS application [87].

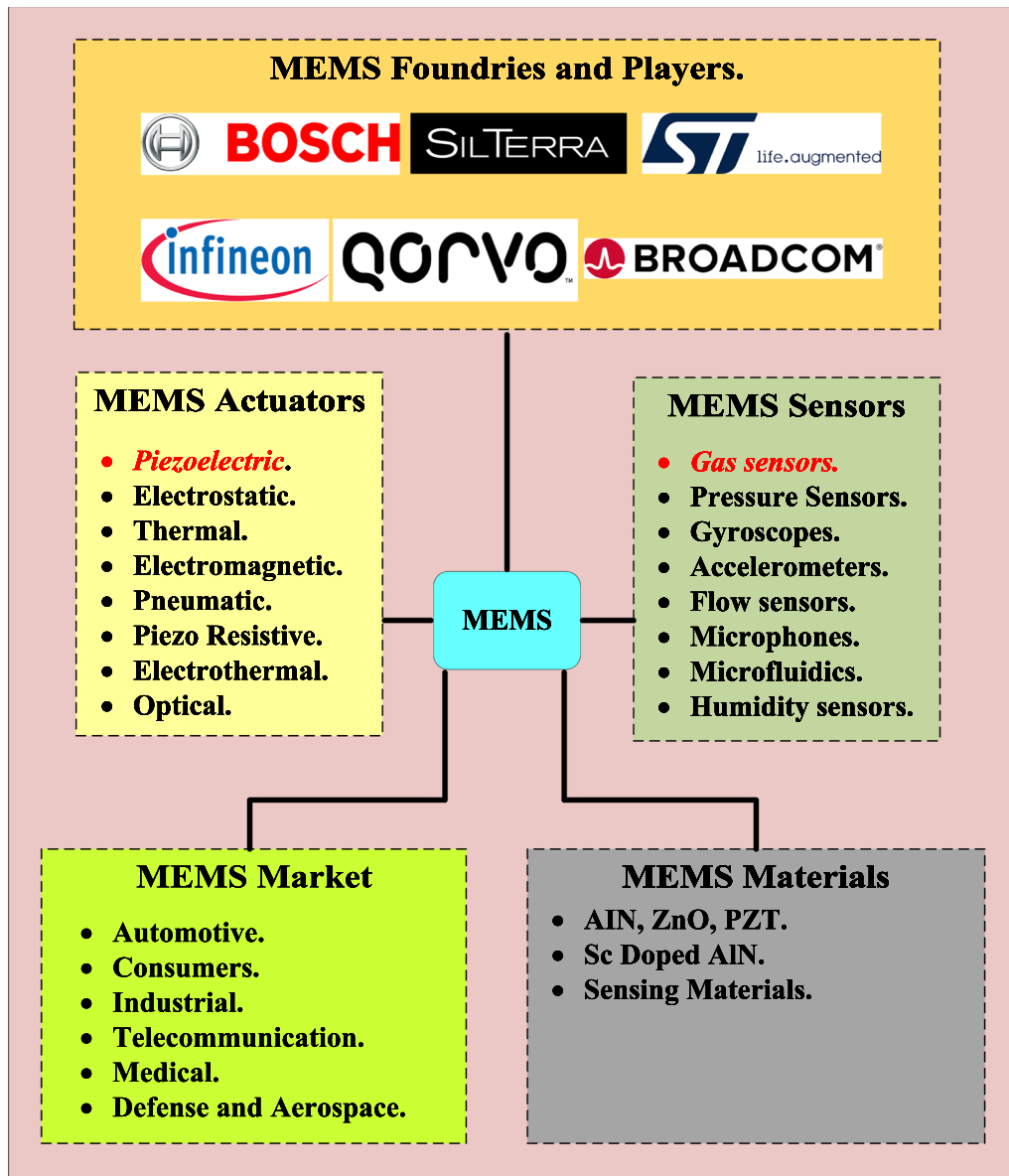


Fig. 1 Overview of the MEMS actuators, sensors, famous foundries, piezoelectric materials and the MEMS market

Figure 1 illustrates an overview of the MEMS actuators and sensors as well as highlighted some MEMS materials, the MEMS market, and MEMS famous foundries.

In the next sections, more details about MEMS gas sensors are illustrated including the performance indicators of the gas sensors as in section "[Gas sensors key performance indicators](#)", the classifications of the gas sensors as in Section "[Classification of gas sensors](#)", as well as the piezoelectric MEMS actuators and sensors transducers as in Section "[Piezoelectric MEMS actuators and sensors](#)", and piezoelectric MEMS resonant modes based on the bulk acoustic wave as in Section "[Piezoelectric MEMS resonant modes based on bulk acoustic wave](#)" including thickness shear mode as in Section "[Thickness shear mode \(TSM\)](#)", lateral extensional mode as in Section "[Lateral extensional mode \(LE\), contour-mode, or lamb wave mode](#)", thickness extensional mode as in Section "[Thickness extensional mode \(TE\)](#)" and flexural

mode as in Section "[Flexural mode \(Flex\) for microcantilever](#)". Furthermore, the piezoelectric MEMS actuators and sensors for gas detection have been demonstrated as in Section "[Piezoelectric MEMS actuating and sensing for gas detection](#)". Additionally, more details of the piezoelectric-MEMS devices have been investigated including the microcantilever as in Section "[Microcantilever](#)", the QCM as in Section "[Quartz crystal microbalance](#)", the SAW as in Section "[Surface acoustic wave](#)", as well as the PMUT as in Section "[Piezoelectric micromachined ultrasonic transistor \(PMUT\)](#)", and the FBAR as in Section "[Film bulk acoustic resonator](#)".

Gas sensors key performance indicators

For high-performance gas sensors, there are several indicators or KPIs that the gas sensors must obtain such as high sensitivity, good limit of detection (LOD), excellent selectivity, fast response, repeatability, fast recovery time, or can be called hysteresis or fast reversibility response, low operation temperature, long-term stability, low cost, small size, monolithically, and robust [88]. Furthermore, gas sensors must meet the industrial demands including less consumption of power, easy production, less production cost, easy operation, etc. [89].

In more detail, the device sensitivity is the ratio of the sensor's output change to the input change, whereas the sensor limit of detection (LOD) can be termed as the sensor's ability to detect the minimum quantity of the targeted gas; therefore, the sensing materials must show high sensitivity in terms of gas adsorption, or in the form of resistance/capacitance changes due to the small amount of the target reaction with the sensing nanomaterials [90]. Secondly, the selectivity of the gas sensors is defined as the ability of the gas sensors to distinguish and identify a specific gas among various types of gas mixtures [91, 92]. Thirdly, the response time of the sensor, can be termed as the time that the sensor takes to generate a warning signal after the targeted gas molecules reached the sensor surface [93, 94]. The excellent gas sensors are always operated with low response time, in other words, low response time means that the sensor will give a super-fast indication and warning signal [93].

Furthermore, the sensor repeatability is addressed as the sensing materials that are applied to the sensor surface should sense the targeted gas over many detection cycles [95]. In addition, the sensor hysteresis or reversibility is defined as whether the sensor sensing materials could return to the original state after adsorbed the target gas. Moreover, the sensor's operating temperature should be as minimum as possible to reduce the power consumption and prevent material damage and defects [96]. Additionally, the sensors should present long-term stability which are defined as the ability of the sensor to produce the same output signals for the same input signals for a long interval of time [97, 98].

Ultimately, the final performance and the LOD of the sensor not only depend on the sensor itself, but also depend on the sensor circuit interface, noise-to-signal ratio, and the quantity of frequency change [99].

Classification of gas sensors

Gas sensors are unique chemical sensors that exhibit variations in at least one of the physical properties of the sensor such as conductance, resistance, absorbance, frequency changes, and temperature variation.

There are various types of techniques have been used for gas detection such as electrochemical sensors, metal oxide semiconductors sensors, capacitance sensors, acoustic sensors, optical sensors, and calorimetric sensors. Gas sensors in this research have been classified into two different categories based on electrical and non-electrical properties variation as shown in Fig. 2.

Over the last years, we have witnessed various gas sensors that are developed based on different transduction methods and different sensing materials. Liu et al. [97] have divided gas sensors into two groups as shown in Fig. 2 based on their sensing transduction methods including the methods that are based on the electrical properties variation such as the metal oxide semiconductors sensors, carbon nanotubes sensors and polymer gas sensors, besides the second group which is based on non-electrical properties variation such as the optics based gas sensors, acoustic gas sensors, and calorimetric sensors.

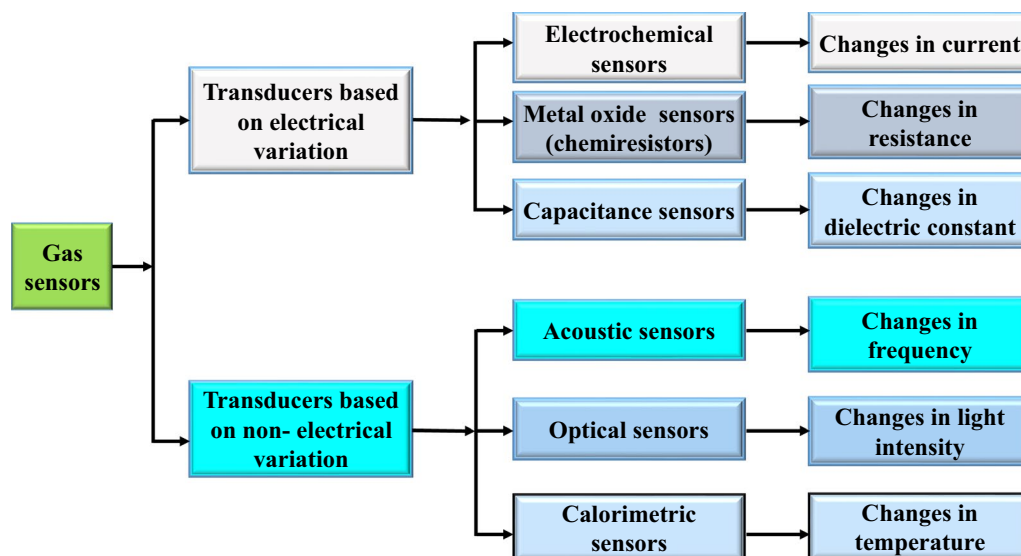


Fig. 2 Classification of gas sensors based on transduction methods [97]

Table 1 summarizes the gas sensors based on their transducer types with brief information about the transduction mechanism and features. Particularly, the table mentioned the common transducers including the electrochemical sensors, gas chromatography, acoustic sensors, optical sensors, as well as the calorimetric sensors. In addition, the gas chromatography and mass spectroscopy (GC-MS) have been used for gas detection and to identify and analyze gaseous molecules with a high capability of generating results rapidly and accurately [100]. However, the GC-MS sensing system requires relatively expensive tools, bulky devices, trained personnel, as well as power-consuming equipment which makes it not suitable for real-time and portable applications [100].

Piezoelectric MEMS actuators and sensors

Actuators are purely analogue devices that provide the transition of real-world signals into electrical signals for communication with humans [13]. In fact, there is a vast variety of microsensors that have been successfully developed and applied in various applications; however, there are only limited applications of the microactuators due to the limitation and insufficient force generated by the small microactuators [101]. Although the most successful microactuators that currently available are dealing with light controlling including optical switches, digital mirror devices, and tunable lenses [102], the piezoelectric and electrostatic microactuators have been shown extremely successful in gas detection applications [103]. Furthermore, thermal actuators have improved significantly and especially in ink-jet printing applications with sharp speed increases thanks to the scaling laws [104]. In addition, extensive development has been contributed to micro-pumps and micro-valves which are always essential for medical implant devices and lab-on-chip applications [105, 106].

In fact, the reduction in MEMS device size is not always preferable due to the huge reduction in the output force of the devices. This can be seen obviously in the electromagnetic microactuators where the size reduction is affecting the output force of the MEMS devices [107]. In addition, the electromagnetic actuators obtained force is a scale to the fourth power of the size; therefore, the electromagnetic actuators are not suitable for small MEMS applications such as gas sensors; however, it is preferable in gigantic projects such as the actuators that are usually used in the satellite [108]. On the other hand, the size issues made the piezoelectric and electrostatic actuations methods as the winners in microsystem applications.

In particular, the piezoelectric actuators are described as the transducers which convert the applied electrical energy into mechanical stress, movement, or strain depending on the type of the piezoelectric materials and the amount of voltage applied [109]. In general, the piezoelectric phenomena are defined as the unique capability or features of some materials -piezoelectric materials- to generate an electrical voltage against any mechanical stress applied on the surface

Table 1 Summary of gas sensors features based on transduction methods

Sensor types	Mechanism	Features	Refs
Electrochemical	The gases diffused at sensing electrode, then the diffused gas get oxidized or reduced.	-Fast response. High sensitivity and good selectivity. Short operation life.	[328]
Gas chromatography	This method based on separation of gases from the gaseous mixture.	- Expensive. Highly sensitive and excellent selectivity.	[100]
Acoustic	The acoustic detection method is determined by measuring the frequency variation of the acoustic sensor after it absorption/adsorption the gas molecules through the sensing layer.	-Good stability. Good response. Good sensitivity.	[11]
Optical	This detection is based on detection the changes in the optical properties such as colorimetric, reflectance, absorbance, luminescence.	-Long lifetime. Good stability. Good response. Good sensitivity.	[329]
Calorimetric	This detection is based on temperature changes because of the oxidation reaction with the gas molecules	-Less selectivity. Low cost.	[330]

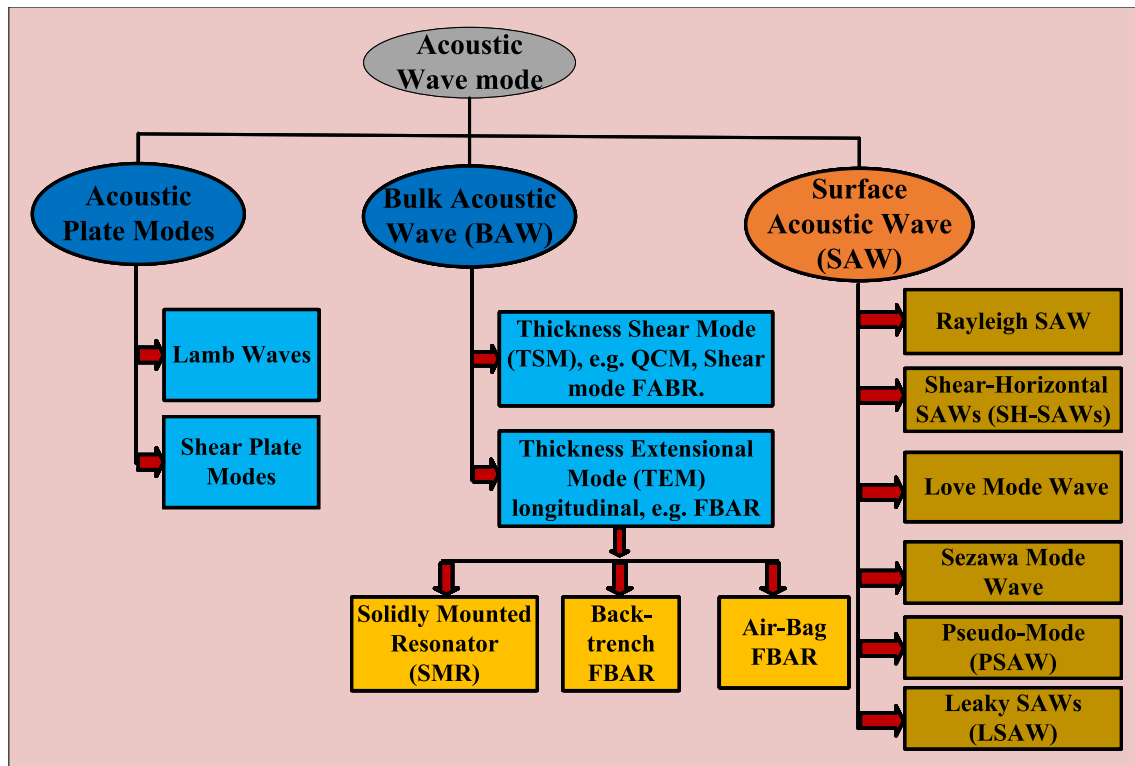


Fig. 3 Classification of different wave modes in two categories: surface and bulk acoustic wave (BAW) and surface acoustic waves (SAW)

of that materials, and conversely where the piezoelectric crystals can produce mechanical deformation, force, and expand when an electrical voltage is applied [11].

In more particular, these piezoelectric devices are classified into two main categories based on the acoustic wave propagation mode which are surface and bulk acoustic wave. In surface acoustic wave devices, the acoustic wave propagates parallel to the surface of the piezoelectric substrate [110]. Moreover, in the bulk acoustic devices, the acoustic wave travels and propagates through the piezoelectric crystal in thickness directions [61]. According to this classification, the QCM, FBAR, PMUT, lamb wave, acoustic plate wave (APW), and shear horizontal-APW are among the bulk acoustic devices [111]; on the other hand, the SAW, Rayleigh SAW, SH-SAW, love mode SAW, Sezawa mode wave, pseudo-mode (PSAW), and Leaky SAW are considered among the surface acoustic devices [112]. The thickness shear mode (TSM) as in QCM and the acoustic plate mode resonators are the most widely used BAW devices; besides, the commonly used SAW devices are the flexural plate wave (FPW) and shear horizontal acoustic wave (SH-SAW). Figure 3 illustrates the different types of acoustic wave modes based on the wave propagation method.

Piezoelectric MEMS resonant modes based on bulk acoustic wave

Section "[Piezoelectric MEMS resonant modes based on bulk acoustic wave](#)" describes the piezoelectric resonant modes based on the bulk acoustic waves that have been developed and utilized in the MEMS sensors. The BAW piezoelectric modes that have been utilized extensively for chemical and gas sensing applications are the thickness shear mode (TSM) as described in Section "[Thickness shear mode \(TSM\)](#)", contour-mode (lateral extensional mode) as presented in Section "[Lateral extensional mode \(LE\), contour-mode, or lamb wave mode](#)", longitudinal mode (thickness extensional mode) as illustrated in Section "[Thickness extensional mode \(TE\)](#)" and the flexural mode as discussed in Section "[Flexural mode \(Flex\) for microcantilever](#)". Figure 4 illustrates the summary of the four different types of the vibration modes.

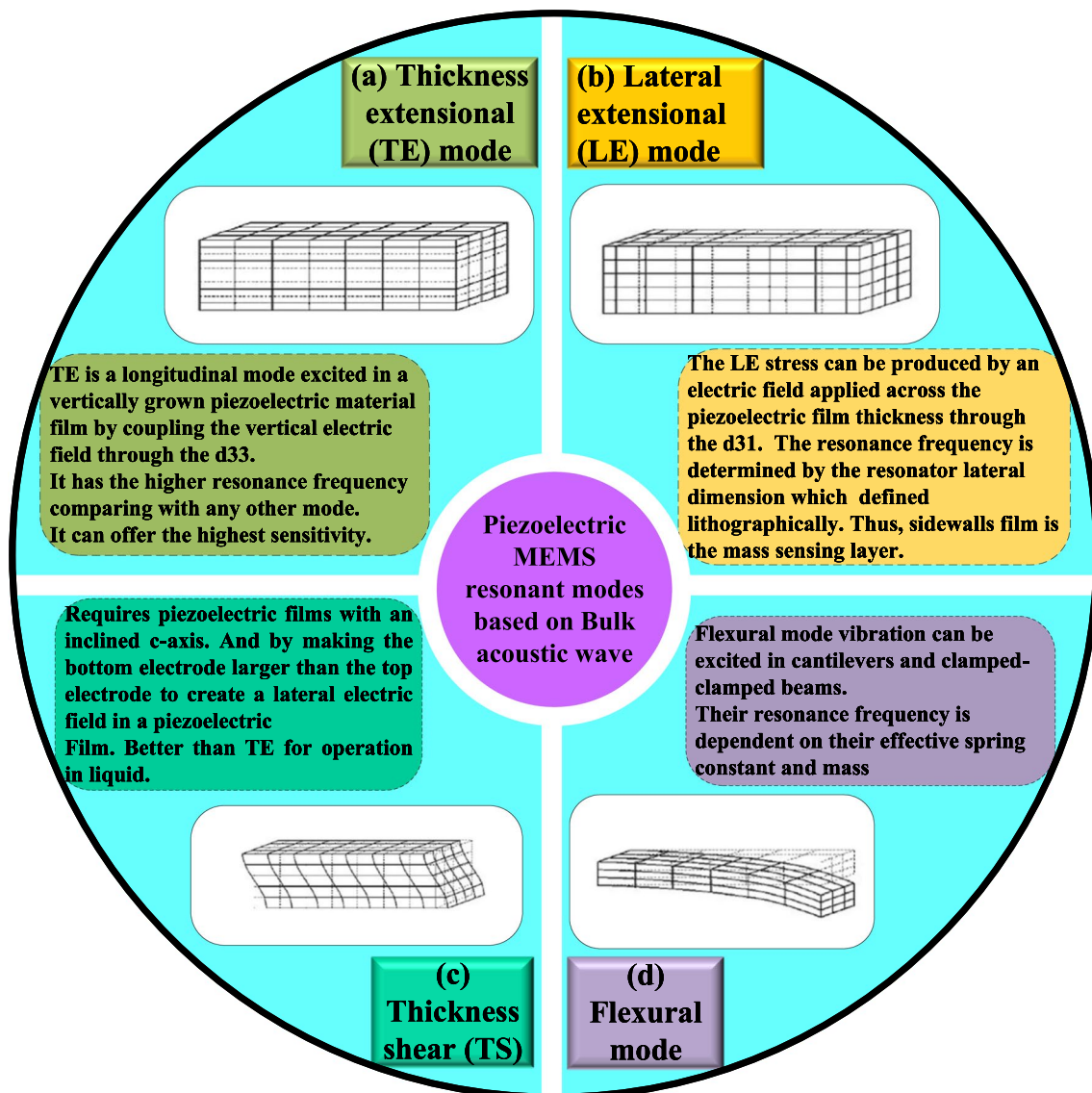


Fig. 4 Typical piezoelectric vibration modes based on bulk acoustic waves, (a) thickness extensional (TE) mode, (b) Lateral extensional (LE) mode, (c) Thickness shear (TS), and (d) flexural mode [119, 136, 289]

Thickness shear mode (TSM)

The thickness shear mode (TSM) resonators use shear acoustic vibrations which are transferred to the surface of the device. The TSM devices are considered the most commonly used bulk acoustic wave (BAW) resonators [113]. Quartz crystal microbalance (QCM) and some kind of film bulk acoustic wave resonators are the most commonly used TSM devices for gas sensing; however, there are two different types of the FBAR which are the longitudinal and the shear mode resonators. The main difference between the shear and the longitudinal FBAR mode is in the sputtering process where the shear mode required a certain type of c-axis angles [114]. The scientists discovered that the pure longitudinal wave can be excited at an angle of 0 and 64, while the pure shear wave can be excited at angles of 42 and 90 [114].

Furthermore, it has been found that the sensors with enhanced sensitivity and high performance for liquid application are the shear mode resonators compared with the longitudinal mode [114, 115]. Since the thickness-shear mode radiates less heat into the liquid than a longitudinal wave and does not cause molecules to move perpendicular to the resonator surface, it is thought to be superior to the thickness extensional mode and longitudinal mode for use in a liquid environment [116]. However, the thickness-shear mode has less quality factor and it is not preferable for gas sensing. Additionally, the longitudinal mode is considered the best option for gas detection sensors [117].

In addition, when the piezoelectric thin film is tilted at angles of 34 and 0, respectively, the longitudinal and shear waves exhibit their highest electromechanical coupling coefficients [112, 118]. The shear mode in thin film bulk acoustic resonators has been demonstrated to be typically triggered by the deposition of a piezoelectric thin film with an angled *c*-axis, where the *c*-axis is not parallel to the thin film plane [119]. To stimulate the shear mode, which causes a shear deformation, a distinct electric field has to be used between the top and bottom sandwiched electrodes. This deformation causes the top and bottom electrode surfaces to move parallel but in opposite directions, creating acoustic waves that travel in the thickness direction [114]. There are other methods for generating a thickness shear mode, such as making the bottom electrode bigger than the top electrode, which creates a lateral electric field in the piezoelectric film [120]. The thickness-shear mode's resonance frequency is dependent on the thickness of the piezoelectric film and the acoustic wave velocity within the piezoelectric materials [121]. Section "Quartz crystal microbalance" describes the thickness-shear mode and its application as gas sensors.

Lateral extensional mode (LE), contour-mode, or lamb wave mode

The lamb wave resonator, or can be called the contour-mode resonator was first demonstrated in 1973 by Toda [122]. In that experiment, the lamb wave resonator was excited by IDTs on unpolarized PZT ceramic plates. Since then, the Lamb wave resonators were extensively investigated for RF and sensing applications. In addition, the Lamb waves technology was brought up again by Piazza et al., around 2005 basically for RF application [123–125]. Subsequently, the development of the Lamb wave resonators was intensively investigated in various applications including the gas sensors. In fact, the structure of the Lamb wave resonator contained both the SAW and the FBAR structure, it can consist of interdigital transducers and FBAR on the cavity or on the SMA structure. Therefore, it has both advantages from these two technologies. It has the IDTs structure so its frequency can be defined by the lithography processes and its suspended structure of the FBAR enables higher quality factor and larger phase velocity [126]. The contour-mode resonator (CMR) or the Lamb wave mode is the MEMS resonator that operates in the transverse direction, of which the resonant frequency is defined and determined by the in-plane dimensions [125]. In this case, however, the resonant frequency is determined by the lateral dimension of the resonator, which can be defined lithographically,

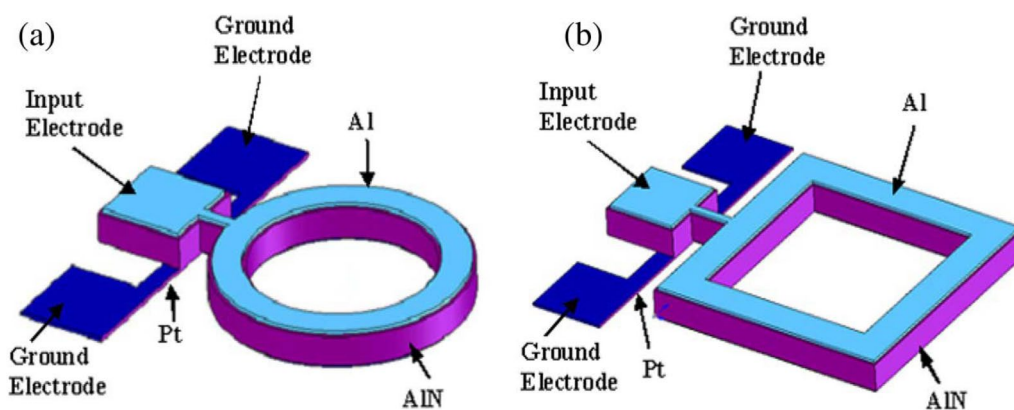


Fig. 5 Micromechanical AlN ring-shaped contour-mode resonators: (a) One port circular ring and (b) One-port square-shaped ring [125]

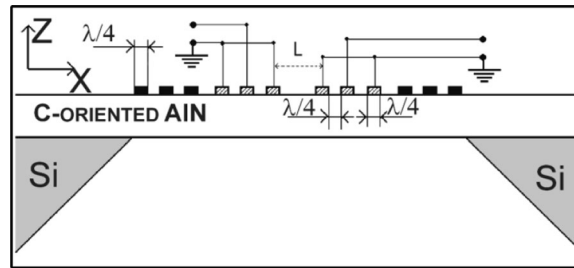


Fig. 6 Schematic of 2-port FPAR Lamb wave resonator [132]

rather than the thickness of the piezoelectric material [127]. Therefore, by using this technology different devices can be fabricated in a single chip with different frequencies [128].

The working principle of the contour mode is depending on the applied AC signal into the device in the direction perpendicular to the surface of the piezoelectric film. Therefore, the electric field supplied across the thickness of the piezoelectric film through the d_{31} piezoelectric coefficient can result in either the contour mode or lateral extensional mechanical stress [129]. Additionally, the resonator structure vibrates in a dilation-type contour mode as a result of this lateral extensional stress, which also excites a longitudinal wave moving laterally [130]. There are two different approaches that can be used to excite the Lamb wave resonators. The first approach is based on the lateral field excitation (LFE) method and the second approach is based on the interdigital transducers (IDT) [126]. In the contour mode, the mass sensing areas are located at the sidewalls of the piezoelectric film as shown in Fig. 5. Thus, the quality factor in a liquid environment can be higher than in a dry one because relatively little longitudinal wave from the piezoelectric sidewalls is transmitted into the liquid [119].

Lamb wave resonators are preferable for biosensors and chemical sensors which operate in the liquid environment due to the physical separation between the analyte and the transducer surface [119, 131]. Thin film plate acoustic resonators (FPAR) have been presented by Arapan et al. [132], for mass sensitivity through Lamb wave technology. The resonators have been theoretically studied, predicated using the finite element method modal, and experimentally verified [132].

Since the Lamb wave resonators have the combined structure of the SAW and the FBAR [133] as presented in Fig. 6; thus, they have the ability to have high resonant frequency and multi-frequency on a single chip, besides high-quality factor, the device can obtain moderate electromechanical coupling coefficient [132]. The phase velocity of the lower-order symmetric Lamb wave mode is up to 10,000 m/s [126]. However, there are some parameters that still need optimization to further reduce the noise in the designed sensors and filters and produce low-lose filters and stable oscillators [133–135]. In addition, the fabrication of these types of resonators is considered not compatible with some common multiuser fabrication technology which is considered one of the obstacles for us to use it in our research.

Thickness extensional mode (TE)

The thickness extensional mode (TE) is considered the most useful mode for the gas sensor application; however, it is not preferable to be used in a liquid environment due to the high damping caused by the liquid when the sensor immersed in fluid in which the liquid absorbs the acoustic energy [136–138]. In fact, the sensor in the TE mode can be excited by coupling the electric field through the d_{33} piezoelectric coefficient using a vertically grown piezoelectric material such as AlN, PZT, and ZnO. The device should have top and bottom electrodes that sandwich the piezoelectric film and an AC voltage is usually applied on these two electrodes which are required to excite the longitudinal resonance. The TE vibration mode always has higher resonance frequency and wave velocity compared with any other modes; therefore, it has a higher sensitivity for mass sensing applications [119, 139]. More information and explanation about the TE mode are presented in Section "Film bulk acoustic resonator"

Table 2 Resonant frequency equations and their range for the four different modes of the piezoelectric vibration based on bulk acoustic waves

Parameters	Thickness shear (TS) mode	Thickness extensional (TE) mode	Lateral extensional (LE) mode	Flexural (Flex) mode
Resonant frequency equation	$f_0 = \frac{1}{2d} \sqrt{\frac{c}{\rho}}$ (1)	$f_0 = \frac{1}{2d} \sqrt{\frac{c_{33}}{\rho}}$ (2)	$f_0 = \frac{1}{2W} \sqrt{\frac{c_{31}}{\rho}}$ (3)	$f_0 = \frac{1}{2\pi} \sqrt{\frac{k}{m}}$ (4)
Range of f_0	5–25 MHz (see Table 3)	800–4.8 GHz (see Table 5)	50–160 MHz	0.03–3.3 MHz

Flexural mode (Flex) for microcantilever

The microcantilevers, clamped beams, membrane, and clamped–clamped beams are all vibrated in the flexural mode by utilizing a thin piezoelectric film to one or both sides of the beam's structure [119]. The flexural mode can be obtained by applying an RF signal across the piezoelectric film, which causes the piezoelectric film to contract and expands depending on the applied frequency. The applying voltage with certain RF causes the entire structure to bend, including the piezoelectric thin film and the attached other materials which form the cantilevers or beams [140]. These piezoelectric beams will be bending and vibrating in flexural mode according to the strength of the applied voltage at the same frequency. If the frequency of the applied voltage is the same as the resonant frequency of the structure, the amplitude of the vibration of the beam will be increased by around Q factor [119]. The cantilevers' resonant frequency is determined by the spring constant and the mass of the cantilevers. The resonance frequency of the cantilevers will be reduced due to the mass added on its surface after the functionalized layer captured the target molecules. The adsorption of the target imposes some stress changes on the cantilevers' surface affecting the stiffness of the cantilevers [141]. Section "Microcantilever" presents more details about the microcantilevers and investigated their application, and Table 2 presents the summary of the parameters of the four different piezoelectric vibration modes based on the bulk acoustic waves.

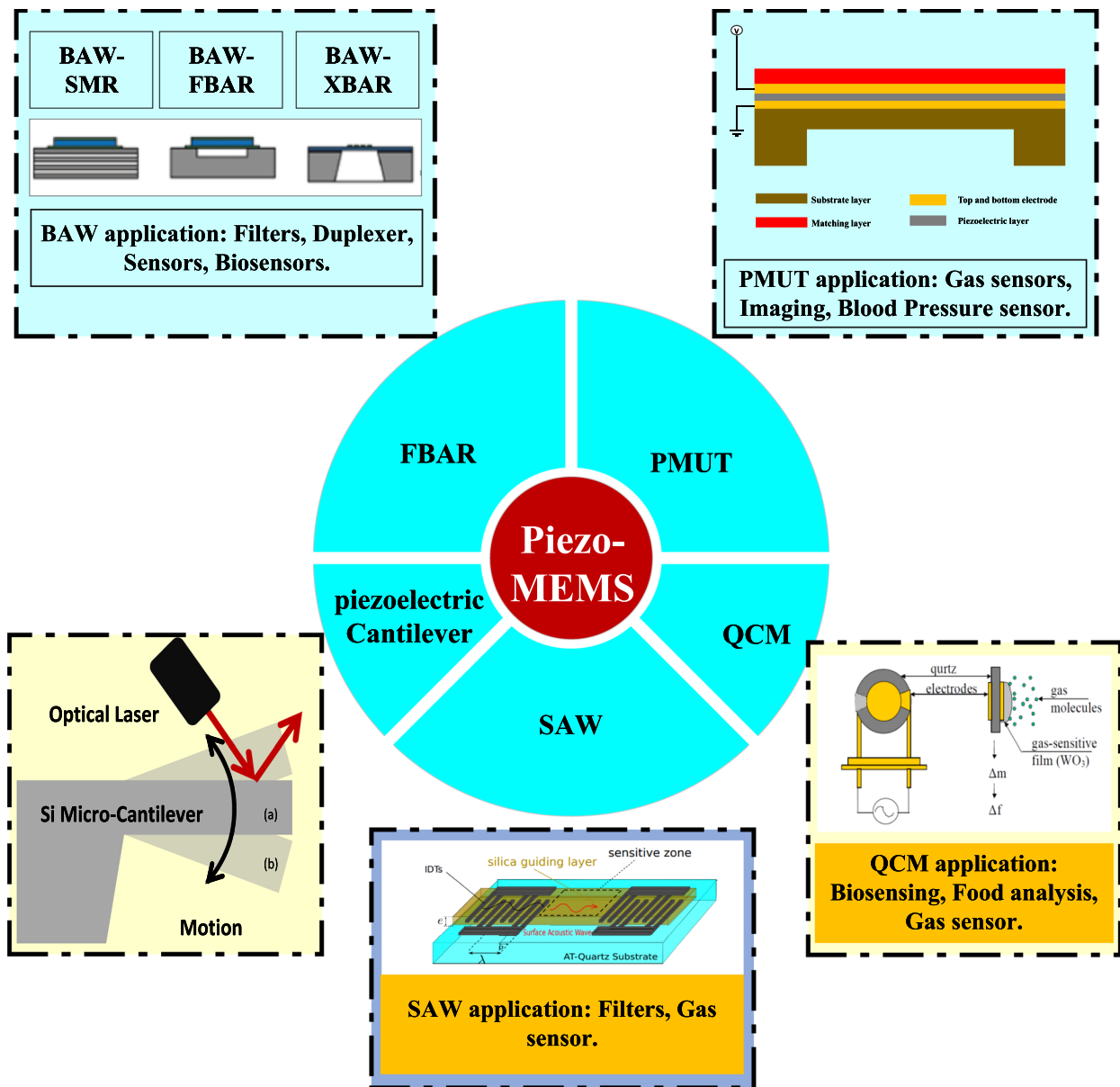
Piezoelectric MEMS actuating and sensing for gas detection

The piezoelectric MEMS actuators and sensors based on the BAW will be investigated in detail and their structures are presented and summarized in Fig. 7.

Section "Microcantilever" introduces the piezoelectric microcantilever, Section "Quartz crystal microbalance" presents the quartz crystal microbalance, Section "Surface acoustic wave" explains the surface acoustic wave resonators for gas sensors application, Section "Piezoelectric micromachined ultrasonic transistor (PMUT)" introduces the application of the piezoelectric micromachining ultrasonic transducers for gas sensors application, and Section "Film bulk acoustic resonator" investigates the working principles of the FBAR extensively.

Microcantilever

Microcantilevers are the most simplified MEMS-based devices [142], which have been used in various applications such as physical, chemical, and biological sensing. They have been used for blood glucose monitoring [143], gas molecules detection, and disease screening [144, 145]. Furthermore, microcantilevers have been utilized in atomic force microscopy (AFM) for the topography imaging of the surface for almost the last four decades [146, 147]. Additionally, the microcantilever beams have demonstrated their capability as highly sensitive, fast-responding sensors with miniaturized size and low fabrication cost which have been used for various applications. Theoretically, the



Structure	Size	Sensitivity	Robust	Power	Frequency
μ Cantilever	Good	Yes	NO	Yes	Low
QCM	NO	Yes	NO	Yes	Medium
SAW	Good	Yes	Yes	Yes	Medium
PMUT	Good	Yes	Yes	Yes	Medium
FBAR	Good	Yes	Yes	Yes	High

Fig. 7 The Schematic for the film bulk acoustic wave, Piezoelectric micromachined ultrasonic transducer, Micro-cantilever, Quartz Crystal microbalance [346], Surface acoustic wave [214]

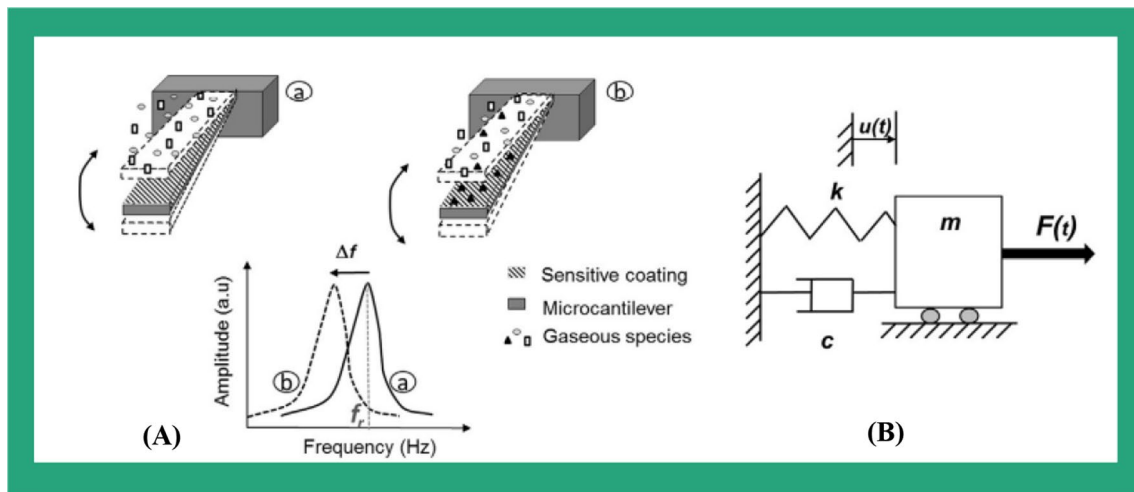


Fig. 8 Illustration of microcantilever utilized as chemical sensors. **(A)** presents the microcantilever detection scheme, **(B)** shows the mass-spring-dashpot system equivalent to the vibrating microcantilever [347]

microcantilever MEMS sensors are responding by bending their structure as shown in Fig. 8 because of the mass changes induced by the adsorption of the analyte molecules on the surface of the cantilevers which lead to a shift in their resonance frequency [142, 148].

The cantilevers have been used in different environmental media such as gaseous, liquid, or vacuum environments [149–151]. The molecules adsorbed on a microcantilever surface can cause vibrations frequency changes and microcantilever deflection [152, 153]. The changes in the vibration frequency can be used for measuring various parameters such as viscosity, density, and flow rate. The deflection is usually proportional to the analyte concentration. Research on resonant microcantilever sensors has focused on enhancing and improving their mass sensitivity by several methods including introducing new material with unique properties, scaling down, or modifying their structural configuration [154, 155].

The measurement of the variation in resonant frequency or the deflection of the silicon beams induced by the adsorption reaction was already described in the literature back in 1968 by Wilfinger et al. [156], who introduced a large silicon cantilever with structures of $50 \times 30 \times 8$ mm. The proposed devices consisted of a silicon cantilever which is mechanically deflected by electrically induced thermal expansion. Additionally, silicon piezoresistive elements were used as readout elements to detect the cantilever stress and provide an electrical output. In more detail, the device was actuated via Joule heating and the piezoresistors were used to measure the beam deflection.

Since then, the cantilevers have been used extensively in various applications, perhaps the most common application of the cantilevers is the force and displacement sensors in the AFM. The first cantilever for AFM was most probably introduced by Binnig et al. [147] back in 1986, who handcrafted the cantilever by cutting thin films of gold foil. Furthermore, the cantilever has been used to actuate by different methods such as electrothermal [157], piezoelectric [158–160], magnetic [161], and electrostatic actuation [162]. After the introduction of the cantilever in 1968 [156], more research has been done to improve and develop the cantilevers to be used as sensors; for instance, Kolesar in 1985 suggested the use of the cantilever structures to be used as electronic nerve agent detectors [163, 164].

Although there are various actuation methods for cantilever vibration that have been used for different applications, this section is only highlighted the piezoelectric cantilevers for chemicals and gaseous molecules detection. Furthermore, the piezoelectric cantilevers are usually actuated by applying an RF signal into the piezoelectric layer using the inverse piezoelectric effect. In the piezoelectric readout method, piezoelectric materials such as AlN, PZT, and ZnO are usually deposited on the cantilever structure. Littrell and Grosh [165] have investigated and developed cantilever-based MEMS using piezoelectric materials for both sensing and actuating.

In addition, Shin et al. [166] have designed, investigated, fabricated, and examined arrays of a piezoelectric microcantilever with various lengths and shapes to optimize their sensitivity and resonance properties. The sol-gel method was used for PZT piezoelectric layer fabrication on a low-stress SiN layer. The natural resonant frequency of the fabricated microcantilever was shown to be in the range of 16–26 kHz. Furthermore, the same authors (Shin et al. [167]) have fabricated a PZT microcantilever transducer for miniaturized gas sensors to detect gas molecules such as volatile

organic compounds. The microcantilever resonance frequency was in the range of 17–29 kHz. The microcantilever surface was coated by polymethyl methacrylate (PMMA) which is well known for its affinity and high sensitivity toward the primary alcohols. The sensors demonstrated obvious changes in the resonance frequency which shifted toward the lower frequency range as the vapor concentration increased. The resonance frequency shift was measured by complex impedance analysis which only uses the electrical signal output from the microcantilever.

Zhou et al. [168] have presented a self-excited piezoelectric microcantilever for Freon gas detection. To develop the microcantilever, theoretical design studies of the device have been done, and the finite element technique has been used to do harmonic analysis on the device. The theoretical and experimental results for the microcantilever's natural frequency are 1.697 kHz and 1.646 kHz, respectively. The microcantilever has been fabricated successfully using bulk-micromachining techniques and solgel spin coating for the PZT piezoelectric layer. The microcantilever sensor has been coated with zeolite nanomaterial as a sensitive layer and the sensor has been characterized for 12 different concentrations of Freon gas ranging from 10 to 500 ppm.

Quartz crystal microbalance

Quartz crystal microbalance devices are an extremely sensitive mass balance based on the piezoelectric effect that can measure micrograms to nanograms levels changes in mass per unit area [169]. In QCM devices, the technology is based on the quartz piezoelectric disk material. The QCM devices use the piezoelectric effect of a thin disk of quartz crystal material placed between two metal electrodes on opposite sides of the disk, as shown in Fig. 9. The overlapping parts of the quartz disk with the electrodes define the active sensing surface [170].

The quartz piezoelectric can be made to oscillate at a defined frequency when an alternating electric field is applied via metal electrodes. The oscillation and the vibration motion of the quartz crystal disk piezoelectric materials established a transverse acoustic wave that can propagate across the crystal materials and reflects again into the surface of the crystal. Therefore, the thickness of the quartz piezoelectric plate defines the quantity of the resonant frequency for the QCM devices which range from 5 to 30 MHz [171]. The QCM devices are also known as thickness shear mode (TSM), and they are considered parts of the bulk acoustic wave devices [172]. The resonant frequency of the QCM can be affected by any mass changes occurring in the electrode surface of the device such as the addition or removal of any small amount of gas molecules. Thus, this range of resonant frequency can be monitored in real time to harvest useful information about the reactions or interactions that occurred on the top electrode of the QCM device such as gas molecular interaction with the sensing layer, oxidation, thin film growth, and material corrosion. Hence, the change in the top electrode mass is linearly related to the changes in the resonant frequency of the QCM sensor where this relationship is expressed by the Sauerbrey equation as shown in Eq. (1) [173]:

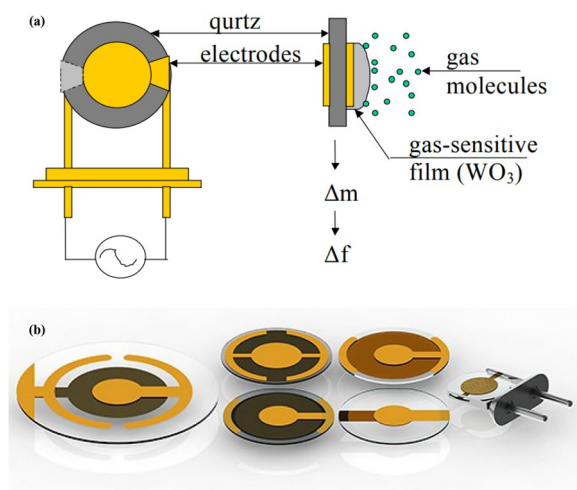


Fig. 9 Schematic of quartz crystal microbalance, (a) presents the QCM for gas molecules detection, (b) shows the different structures of the QCM [346]

$$\Delta f = -\frac{2f_0^2}{A\sqrt{\rho_q\mu_q}}\Delta m \quad (1)$$

where Δf is the change of the resonant frequency in Hz, f_0 is the resonant frequency of the fundamental mode, Δm is the mass change in (g), A is the piezoelectrically active crystal area which is between the two metal electrodes in (cm^2), ρ_q representing the quartz crystal density which is equal to 2.648 g/cm^3 , and the μ_q representing the shear elastic modulus of the quartz which is equal to $2.947 \times 10^{11} \text{ g} \cdot (\text{cm}^{-1}) \cdot (\text{s}^{-2})$ [174].

A QCM gas sensor was used for the detection applications of hazardous gases at room temperature by Alev et al. [175]. The surface of the QCM sensor has been deposited by Cu doped with ZnO nanorods (NRs). This sensitive nanomaterial was successfully synthesized from Cu-doped and pristine ZnO nanorods using two-step electrochemical deposition technique, which was optimized in this experiment to get highly ordered ZnO nanorods. The QCM-fabricated gas sensor was tested to detect several gases including H_2S , NO_2 , HCN, isopropyl alcohol, ethyl acetate, xylene, and toluene. In this experiment, the results shown that the process of Cu doping with ZnO nanorods has obviously enhanced the sensor sensitivity at room temperature, especially for H_2S and HCN gases. The variation of the Cu doping ZnO concentration has shown that the 1% concentration of the Cu doping ZnO nanorods presented the highest sensor response compared with 3% Cu doped with ZnO, where this increment in the sensor response was justified by the enhancement of the physisorption properties of the NRs surface.

Furthermore, Trajcheva et al. [169] reported the investigation of the QCM gas sensor sensitivity coated with graphene nanoribbons (GNR)/ polymer hybrid nanocomposite for several hazardous gas detection. The GNRs are narrow strips of graphene that are characterized to be in one-dimensional morphology with significantly excellent surface properties, that can offer a huge number of functional groups. The GNR has been mixed with a cheap polymeric material to obtain a highly sensitive nanocomposite. The GNR/polymer nanocomposites have been produced for the first time in this experiment by using the advantages of polymerization in the dispersal media to act as green synthesized material. The interaction between the GNR/polymer nanocomposite was formed by established covalent bonding between the phases of both materials, this type of bonding is responsible for boost of the strong thermal and mechanical in the nanocomposites. This QCM has been deposited with GNR/polymer nanocomposites and exposed to various gases including NH_3 , N_2O , and CO in a different amount of concentration range from 70 to 1000 ppm. The developed QCM sensors were characterized at room temperature for three cycles of gas adsorption and desorption and the large number of responses of response in a short time. The QCM sensors have shown excellent performance, especially in the reproducibility of the sensor for the investigated three cycles.

The extraordinary improvement in the sensor performance was attributed to the huge number of functional groups that have been created between the polymer and GNR where these functional groups and the uniqueness of the nanocomposite morphology that offers numerous adsorption agents. The selectivity of the QCM sensor with GNR/polymer nanocomposites was investigated for the three gases and the sensors showed excellent selectivity toward NH_3 gas compared with CO and N_2O . The authors reported that the selectivity of the sensor was due to the interaction between the NH_3 and the nanocomposites by Wan der Waals forces and hydrogen bonding that only formed between the nanocomposites and the NH_3 gas whereas, the other two gases was interacted exclusively by the van der Waals interactions [169].

In addition, QCM sensors' performance has been enhanced by utilizing highly functionalized reduced graphene oxide (rGO) to detect carbon dioxide at room temperature by Gupta et al. [176]. The thin film rGO was chemically synthesized by chemical reduction in graphene oxide using an Ascorbic acid green agent. In this experiment, the rGO was optimized using three different concentrations of the ascorbic acid reduction agent which are (25, 50, and 100 mg). Three different thin films were prepared and analyzed using several characterizations such as SEM, TEM, XRD, FTIR, XPS, RAMAN, and four-point probe measurement. The rGO thin film with 25 mg of reduction agent showed excellent sensing properties in terms of sensing and time of recovery with enhanced repeatability for CO_2 detection with a variation of 500–50 ppm at room temperature. The QCM gas sensors sensitivity has been investigated for 500 ppm CO_2 gas which shows 50 Hz μg at room temperature. The response and recovery time of the QCM sensors was reported to be 26 and 10 s, respectively [176].

Furthermore, QCM devices for gas sensors application have been used extensively along with the development of nanomaterials which has enhanced the sensitivity and selectivity of the sensors. A research paper published by Chen et al. [177] demonstrated a unique method for depositing graphene oxide and cuprous oxide ($\text{GO}/\text{Cu}_2\text{O}$) nanocomposites on the surface of the QCM via a layer-by-layer self-assembly technique. This work was used for trimethylamine gas detection with low concentrations under 5 ppm. The response of the QCM sensor has been increased linearly with the gas concentration. The authors reported that the QCM gas sensors presented good selectivity, sensitivity, stability,

Table 3 Summary for QCM gas sensors

Piezoelectric materials	Device frequency (MHz)	Sensing layer	Target	LOD (ppm)	Frequency shift (Hz/ppm)	Response time (s)	Recovery time (s)	Temp	Year	Ref
AT-CUT	25	PAAM/MWCNTs.	Formaldehyde.	0.5	3	80	100	RT	2021	[331]
AT-CUT	10	Cu-doped ZnO NRs.	H ₂ S	6.6	68	n/g	n/g	RT	2020	[175]
AT-CUT	10	rGO	CO ₂	50–500	50	26	10	RT	2021	[176]
AT-CUT	10	MOF	CO ₂	400–500	n/g	n/g	n/g	RT	2018	[179]
AT-CUT	9	(ZIF-8)	CO ₂	1.000.000	217	10	n/g	RT	2018	[215]
AT-CUT	9	Graphene oxide	Formaldehyde	1.7	22.9	60	n/g	RT	2016	[332]
AT-CUT	9	ZIF	CO ₂	n/g	n/g	n/g	n/g	RT	2018	[333]
AT-CUT	8	PEI/MWCNTs	Formaldehyde	6	0.82	114	127	RT	2015	[334]
AT-CUT	8	SnO ₂ /Polydopamine	Formaldehyde.	0.5–50	12.2	25	38	RT	2021	[335]
AT-CUT	5	polymer/GNR.	NH ₃	70	106	1800	n/g	RT	2021	[169]
AT-CUT	n/g	GO/Cu ₂ O.	Trimethylamine.	5	15.2	20	n/g	RT	2018	[177]

n/g = Not Given

and reversibility during the 60 days of investigation. The limit of detection (LOD) in this experiment was illustrated to be 230 ppb under room temperature for trimethylamine gas using QCM. The gas detection mechanism using GO/Cu₂O nanocomposites was demonstrated as an adsorption–desorption process that was carried out via the interaction called the hydrogen bonding between the carboxyl functional groups on the surface of the GO and the trimethylamine gas molecules. Furthermore, the layer-by-layer self-assembled method has enlarged the surface area of the p-n junction of GO/Cu₂O which enhanced the physical adsorption of trimethylamine gas molecules [177].

Fauzi et al. [178] summarized the recent progress in the development of QCM devices that are coated with graphene materials and graphene composite nanomaterials which are used for gas and humidity-sensing applications. The min review paper mainly focused in the recent advances of the QCM gas and humidity sensors' performance, especially the characterized of the devices that are coated with pristine graphene, graphene oxide, reduced graphene oxide, and different graphene composite materials such as graphene–metal oxide composite, polymer, chemical, and other carbon-based materials. The report addressed the QCM sensors' challenges for sensor future development [178]. Table 3 summarizes some of the recently highlighted research for the development of the QCM for gas sensor application.

Surface acoustic wave

SAW technology produces highly sensitive devices for chemical detection in both gaseous states as well as liquid environments [179]. In 1965 [180] SAW technology was introduced for the first time by White and Voltmer who reported the generation of surface acoustic waves by utilizing interdigitated pair of electrodes called interdigital transducers (IDTs) which were fabricated on a quartz piezoelectric surface and actuated by applying RF voltage [181]. In that contribution, the SAW waves were generated by applying a voltage signal to the fabricated IDTs electrodes on the surface of the devices. Since then, SAW technology has been extensively investigated and developed for wide applications [182].

Wohltjen and Dessy in 1979 [183] used SAW technology for the first time for organic gas detection by coating a sensitive sensing layer on the top surface of the SAW device. This breakthrough attracted the researchers' attention and a variety of SAW devices has been reported for gas detection. The sensitivity of the SAW sensors highly depends on the sensitivity of the sensing film, coated on the top surface of the device [184]. The sensing layer must possess the capability of adsorbing certain types of gases and does not react with other gases which determined the selectivity of the gas sensors [185].

In addition, the SAW device transducer mainly determines the sensitivity of the SAW gas sensors, while the coated nanomaterial usually determines the selectivity and specificity of the sensor [186]. The SAW sensors technology is considered one type of gravimetric transducers which are relied on Sauerbrey's classical theory that has been published in 1959 [173]. The Sauerbrey contribution has described the relationship between the weight and the change in the resonant frequency of piezoelectric materials.

Surface acoustic wave devices have been developed in the early stages mainly for certain applications including signal processing [187, 188], resonators, actuators [189], frequency filters [190, 191], and others [192, 193]. However, in the last few decades, there are a significant increase in the SAW for gas, chemical, and biochemical detection application [182]. The SAW sensors have offered several advantages which determine by the piezoelectric transducers such as wired and wireless operation, fast response, ultra-high sensitivity, small size, low cost, and compatibility with modern fabrication technologies [194].

In addition, the SAW sensors can provide more extra advantages which rely upon the proper selection of the coated sensing layer including excellent selectivity, reversibility, stability, linearity, and fast response [195]. The SAW sensors performance determines by some main factors including the piezoelectric substrate, the material of the sensing layer, and the interdigital transducers (IDTs). The SAW gas sensors are intended to address the rapidly increasing need for high-performance gas and chemical sensors in all applications, including pollution monitoring, military, and industrial [196], industries, volatile organic chemicals (VOCs) [110, 197], and detection of other various toxic gases [198, 199].

The SAW device sensors' work basis on variations in acoustic wave propagation, that are influenced by interactions between the waves and the environment nearby, such as the target gas or the surface layers. In fact, the SAW acoustic waves depend on the propagation medium characterizes, elastic stiffness, mass density, and electric–dielectric behavior of the piezoelectric materials. There are various types of SAW devices that operated differently. The SAW devices can operate between a few MHz and a few GHz where this frequency is higher than the QCM devices; therefore, the sensitivity of the SAW is considered higher compared with the QCM piezoelectric sensors. A “delay line” SAW sensor is considered fundamental to the SAW devices. It consisted of IDTs deposited on both sides of the piezoelectric substrate where one of them performs as input and the other as output IDT. The IDTs are made from periodic metals that are typically shaped like two combs that cross over from opposite sides. The surface between the two IDT as shown in Fig. 10 is the sensing area where the sensing material is deposited for target detection.

The interaction of the sensing layer and the target gas or chemical in the region between the input and output IDTs causes the time difference between the input and output signals. The length of the sensitive layer as well as the velocity of the SAW material influences how long the output signal is delayed. The presence of the target or analyte in the sensing layer, in particular, changed the acoustic waves' phase velocity, attenuation, and amplitude.

Hence, these variations in the output electrical signal at the output IDT could yield some useful information [200]. SAW wave propagation in the piezoelectric layer can produce both electrical potential and mechanical deformation [201]. The mass loading on the surface of the sensor and the elastic and viscoelastic are the mechanical deformation caused by the interaction between the sensing layer and the targeted analytes [59]. In addition, these effects are called the acoustoelectric effects which are the effects that result from the interaction between the presented targeted analyte in the sensing layer and the electrical field associated with the SAW waves [202].

Moreover, there are basically three common modes of SAWs devices that are extensively utilized for gases and chemicals detection, namely Rayleigh wave mode [203], Lamb wave mode [204], and shear horizontal wave mode (SH-SAWs) [205]. In addition, most of the reported SAW gas and microfluidic sensors are based on the Rayleigh waves mode [206, 207], whereas the shear horizontal and Lamb wave SAWs are only suitable for gas sensors, but they are not able to perform the detection in the microfluidic or liquid-based sensing environment due to the fact that the wave propagation in the shear horizontal mode and its displacement is only parallel with the substrate surface, which inhibits the wave vibration into the liquid on the surface [181]. The Rayleigh waves are type of surface waves that travel near the surface of solids in both longitudinal and transverse motions [208]. In Rayleigh wave mode, the SAW propagates at the speed of sound on the crystal. However, the amplitude of these waves decreases exponentially with the increase in the distance from the solid's surface. The Rayleigh waves were predicted by Lord Rayleigh

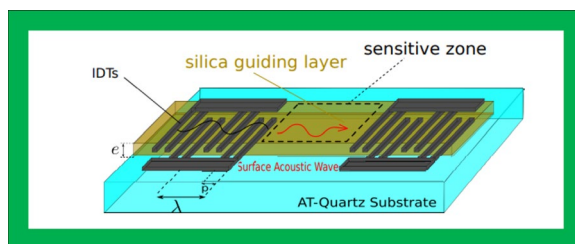


Fig. 10 Structure of a surface acoustic wave based on a delay line built on an AT-cut quartz substrate, produced by [214]

in 1885 [206], after whom they were named. In more detail, the Rayleigh SAW sensors are creating an out-of-plane elliptically polarized surface wave caused by the acoustic energy near the piezoelectric substrate surface [209]. The resonant frequency of the SAW devices [210] is calculated by Eq. (2):

$$f = \frac{v}{l} \quad (2)$$

where v is the velocity of the wave for the certain substrate material, and the l is the wavelength. In fact, the perturbation theory describes the changes in the resonant frequency which will be affected by the mass changes caused by the gas adsorption [211]. Furthermore, the SAW resonant frequency changes that occurred after the gas or analyte absorbed by the coated layer can be expressed by Eq. (3) [212, 213], where the absorbed gas considered as non-piezoelectric, non-conductor, with a density of p , and a thickness h . Equation (3) can be expressed as:

$$\Delta f = (k_1 + k_2)f_0^2 \rho h - k_2 f_0^2 \rho h \frac{4\mu}{v_0^2} \left(\frac{\lambda + \mu}{\lambda + 2\mu} \right) \quad (3)$$

where f_0 is the unperturbed resonant frequency of the SAW oscillator, which is determined by Eq. (2), and it is affected by the propagation velocity of the SAW and the number of the comb fingers that fabricated on the surface of the piezoelectric substrate; k_1 , and k_2 are the coupling constants which can be determined by the SAW device different displacement components; v_0 is the unperturbed velocity of the SAW waves in the piezoelectric substrate; μ and λ are the shear modulus and the Lamé constant of the layer that have been generated after the gas adsorption. However, this formed layer that has been created by the adsorbed or absorbed gas is very thin layer which made the second part of the equation close to zero. Therefore, the second term of the equation depends on the acoustic wave coupled into the layer whereas, the first part of the equation will be remained to be calculated which represents the SAW resonant frequency changes caused by the mass loading on the surface of the SAW. Therefore, Eq. (3) can be simplified as expressed Eq. (4):

$$\Delta f = (k_1 + k_2)f_0^2 \rho h \quad (4)$$

where the ρh is the new density of the layer that has been formed after the gas adsorbed [212, 213]. These equations have been developed theoretically and proven experimentally by Wohltjen, who investigated in detail the relationship between the interaction of the vapor molecules and polymeric coating films on the surface of the SAW device [212]. Furthermore, Djoumi et al. [214] developed a real-time mass sensor using SAW for PM10 and PM2.5 mass concentration measurement. They produced SAW sensors with a working frequency of 125 MHz based on love waves delay lines mode where the waves propagate on AT-cut quartz substrate as presented in Fig. 10.

Recently, Palla-Papavlu et al. [186] have published a review paper that presented the latest progress development in the sensing layer nanomaterial including polymers, and functionalized carbonaceous materials, organic salts, and self-assembled monolayers for SAW sensors. The survey paper reported the synthesis processes of the functionalized CNTs and graphene that have been used to enhance the sensitivity of the SAW and other acoustic sensors. Furthermore, the sensing layer coating techniques and methods have been illustrated including physical, chemical, spray coating, ink-jet printing, and other surface modification methods. The authors have compared and highlighted some of the best routes for the enhancement of the acoustic sensors' performance that is used for dangerous compound detection. In fact, there are many effects have been focused to enhancing the performance of the SAW sensors by either improving the current nanomaterials sensitivity through the modification of their surface morphology and attachment of functional groups that will be binding with the analyte or by synthesis of entirely new sensitive materials [186].

In addition, Jagannath Devkota et al. [215] have designed and fabricated SAW delay line sensors for CO₂ and methane detection at the ambient condition at operating frequency of 436 MHz. The sensitivity of the SAW sensors was enhanced by directly coated zeolitic imidazole framework-8 (ZIF-8) metal-organic framework (MOF) on the surface of the SAW devices. The fabricated SAW sensors were tested for several gases detection, and the devices were able to detect the changes in the concentration of CO₂ and NH₄; however, the sensors' sensitivity toward CO₂ was much higher compared to NH₄, which was due to the CO₂ higher adsorption potential and their heavier molecular weight.

The SAW gas sensors have shown full reversibility and repeatability which were confirmation of the physisorption of the gases into the MOF indicating the physical bonding of the gases molecular with the surface of the MOF which provides high stability of the sensors. This research confirmed the potential and capability of the ZIF-8 in adsorbing carbon dioxide gas molecules. Furthermore, the authors have published another research paper [216] for wireless and passive

SAWs gas sensors using the same sensing layer which was a nanoporous metal–organic framework, specifically the ZIF-8 sensing film for carbon dioxide and methane gas detection at ambient conditions; however, the sensitivity of the reflective delay line SAW gas sensor was enhanced by increasing the resonant frequency from 436 MHz (8 μm periodicity) to 860 MHz (4 μm periodicity) [215].

The increase in the operating frequency has enhanced the sensor sensitivity at least four times and the detection limit of the higher frequency devices was estimated to be 0.91 vol%; thereby, the enhancement in the sensor sensitivity by higher frequency devices is explained and confirmed that the acoustic devices are frequency dependent. In this published paper, the design, fabrication, characterization, and parameters classification [216].

Furthermore, the sensitivity, stability, and selectivity of SAW gas sensors were enhanced by the integration of treated lead sulfide (PbS) colloidal quantum dots (CQDs) into the surface of the SAW devices [217]. In that research, the authors investigated the utilization of nanomaterials for SAW gas sensors' performance enhancement for NO₂ detection at room temperature. The SAW sensors were coated with untreated PbS CQDs which were directly deposited on the delay line SAW devices using spin coating techniques followed by chemical treatment. The experiments illustrated the responses, recovery time and the frequency shift of the SAW sensors using the treated and untreated PbS CQDs nanomaterials. The results were shown that the sensors with untreated nanomaterials shown response and recovery time of 487 s and 302 s with a negative frequency shift of 2.2 kHz.

In contrast, the treated nanomaterials presented dramatic improvement in the sensitivity, selectivity, stability, response, and recovery time at room temperature with a sharp increment in the frequency shifts. In particular, the sensor response and recovery time were reported to be 45 s and 58 s with positive frequency shifts of 9.8 kHz, respectively. The improvement in the treated nanomaterials might be caused by the trapping of the NO₂ molecules into the porous film which increases the film stiffness [217].

Tang et al. [218] have reported SAWs gas sensors for NH₃ gas detection using several sensing layers such as pristine SiO₂, TiO₂, and composite SiO₂ – TiO₂ films. The thickness of the sensing layers was 200 nm and coated on the surface of quartz acoustic wave sensors using solgel and spin coating techniques. The performance and mechanism of the SAW sensors were systematically investigated. The experiments had shown that the sensors made of TiO₂ and SiO₂ – TiO₂ films exhibited positive frequency shifts toward NH₃ whereas only SiO₂ sensing layer presented a negative frequency shift toward the gas. The authors illustrated that the negative frequency shifts were mainly caused by the mass increase in NH₃ gas into the surface of the SAW sensors.

Table 4 Summary of related SAW sensors for gas detection

Piezoelectric materials	Device frequency (MHz)	Sensing layer	Target	LOD	Frequency shift	Temp	Ref
Y-Z LiNbO ₃ delay lines	860	ZIF-8	CO ₂	0.91 ppm/vol.	1.11 rad.	RT	[216]
Y-Z LiNbO ₃ delay lines	860	ZIF-8	CH ₄	16.6 ppm/vol	4.58 rad.	RT	[216]
Y-Z LiNbO ₃ delay lines	436	ZIF-8	CH ₄	7.01 ppm/vol	0.136 rad.	RT	[215]
Y-Z LiNbO ₃ delay lines	436	ZIF-8	CO ₂	0.38 ppm/vol	1.396 rad.	RT	[215]
ST-cut quartz.	434.15	Nickel-Alanine-Graphene.	CO ₂	200 ppm.	2.07 Hz/ppm	RT	[336]
ST-cut quartz.	433.8	AuNR.	VOCs	2.64 ppm	n/g.	RT	[110]
ST-cut quartz.	433	Graphene.	DMMP	10 ppm	–1.4 KHz/ppm.	25–100 °C	[337]
ST-cut quartz.	200	GO Nanofilm.	CH ₃	500 ppb	620 Hz/500 ppb.	RT	[338]
ST-cut quartz.	200	Bi ₂ S ₃ nanobelts	NO ₂	1.2 ppm.	2 kHz/10 ppm.	RT	[339]
ST-cut quartz.	200	ZnO-Al ₂ O ₃ .	H ₂ S	10 ppb.	500 Hz/10 ppb.	RT	[340]
ST-cut quartz.	200	boehmite.	NH ₃	10 ppm	1540 Hz/10 ppm	RT	[341]
ST-cut quartz.	200	CuO-Al ₂ O ₃	H ₂ S	5 ppb	15 KHz/1 ppm.	RT	[342]
ST-cut quartz.	200	Nitrogen doped Diamond.	NH ₃	100 ppb	0.65 KHz/100 ppb.	RT	[343]
ST-cut quartz.	200	SiO ₂ , TiO ₂ .	NO ₂	16 ppm.	112 KHz/40 ppm.	RT	[218]
ST-cut quartz.	200	PbS.	NO ₂	10 ppm.	9.8 KHz/ppm	RT	[217]
ST-cut quartz.	99.5	ZnO.	NO ₂	16 ppm.	112 KHz/40 ppm.	RT	[344]
ST-cut quartz.	198.98	CuO.	H ₂ S	500 ppb.	–1200 Hz/500 ppb.	RT	[345]

n/g = Not Given

In contrast, the positive frequency shift was basically associated with the hydroxyl groups (-OH) condensation on the sensing layer film due to the NH_3 exposure; thereby, this reaction is making the film more stiffer and lighter [218]. The fabricated SAW sensors' performance was characterized under the effect of humidity, and it has been demonstrated that the humidity played a significant factor in the coated SAW sensors' performance. Additionally, studies in the literature exhibited that the performance of the SAW gas sensors was dramatically enhanced due to the utilization of highly sensitive thin films as it has been proven in this research [218] that the $\text{SiO}_2 - \text{TiO}_2$ thin film had increased the sensitivity of the SAW gas sensors for NH_3 gas to lower concentration (1 ppm) with a frequency shift of 2 kHz and it also shown fast response, excellent selectivity, stability, recovery, and reproducibility [218].

Furthermore, the summary of the recent research for the development of the SAW for gas sensor application is presented in Table 4.

Piezoelectric micromachined ultrasonic transistor (PMUT)

The PMUTs are MEMS-based piezoelectric ultrasonic transducers usually used for acoustic imaging of the surrounding environment such as in the medical imaging [219–221], in the automotive [222], fingerprint devices [223–225], fluid density sensing [226] and for gas sensor applications [227]. Although the PMUT and the FBAR are similar in their structure, the PMUT devices are unlike the FBAR solid-based piezoelectric transducers, where the FBAR devices are based on the thickness motion of the piezoelectric plate; however, the PMUTs are based on the bending motion of a thin membrane coupled with a piezoelectric thin film. A typical structure of the PMUT is shown in Fig. 11. Typically, the PMUT has a single piezoelectric layer between the top and bottom electrodes, the electrode should have a specific parameters such as high conductivity. Furthermore, the PMUT can be used as gas sensors by functionalized the top electrode by sensing materials. The sensing materials have significant impact on sensor sensitivity and can influence sensor resonance frequency. PMUT gas sensors offer the ability to overcome some of the problems that other types of gas sensors have, such as power consumption, where the PMUT has the ability to operate by a lower voltage. In addition, the PMUT gas sensors always contained a large top electrode surface which provides enough space for the sensing materials [227].

The working principle of the PMUT gas sensors is mainly determined by the device structure, piezoelectric material thickness, and parameters. For instance, the resonance frequency for a basic PMUT element with one rectangular structure and PZT/Si layered membrane with fully clamped boundaries can be calculated by Eq. (5) by Ref [228, 229]:

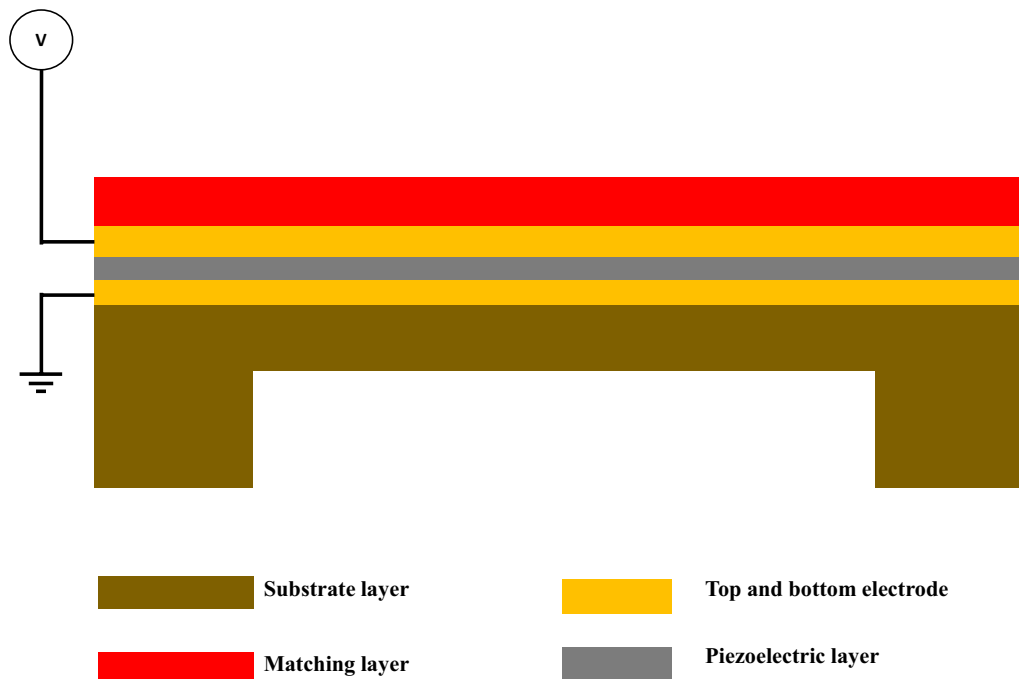


Fig. 11 The typical schematic view of the piezoelectric micromachined ultrasonic transducer (PMUT) [227]

$$f_0 = \frac{0.494t}{w^2} \sqrt{\frac{E}{\rho(1-\nu^2)} \left[1 + \frac{2}{3} \left(\frac{W}{L} \right)^2 + \left(\frac{W}{L} \right)^4 \right]} \quad (5)$$

where L is the length, w is the width, t is the thickness, E is Young's modulus, ρ is Poisson's ratio, and ν is the density of the material. Equation (5) has clearly highlighted that the resonance frequency of PMUT sensors is primarily governed by the geometry, radius, and thickness of both the piezo-material thin film and the electrodes. Therefore, any modification or defect in these parameters will definitely affect and alter the PMUT resonance frequency. In addition, the operating frequency of the PMUT is typically known to be proportional to Young's modulus and inversely proportional to the density of the rectangular membrane.

Sun et al. [229] have produced a very sensitive humidity sensor utilizing the PMUT array with a surface functionalized using a graphene oxide thin film. The PMUT sensors have been proposed, fabricated, and tested for humidity sensing where the fabricated sensors showed high sensitivity, good stability, and fast response. Furthermore, Nazemi et al. [227] reported the utilization of the PMUT and CMUT as mass sensors with an extensive investigation of their working principle, device structures and configuration, fabrication processes, critical design parameters, and the resonant frequency changes. The PMUT devices currently are used extensively in ultrasonic imaging production comparing with their application as gas and chemical sensors [222, 230].

Film bulk acoustic resonator

Over the last two decades, there has been an increased interest in developing and producing high-frequency devices (from sub-GHz to tens of GHz range) such as bulk acoustic waves (BAWs) resonators which have been used as filters [231–236], duplexers [237–239], multiplexers [240, 241], gas sensors [242–245], and chemical biosensors [71, 246, 247]. The film bulk acoustic wave devices are one of the BAW resonators which consisted of a piezoelectric layer usually zinc oxide (ZnO), aluminum nitride (AlN), or lead zirconate titanate (PZT) sandwiched between two metal electrodes to which microwave (RF) signal is applied [245].

The first FBAR device had been disclosed in 1980 by Lakin and Wang [248] and several other groups published similar research during approximately same time [249, 250]. Additionally, FBAR is considered as a development of the previously discovered quartz resonator that has been first reported by Sliker and Roberts in 1967 which consisted of a piezoelectric CdS film on a quartz substrate [251]. However, Lakin and Wang reported a new and unique form of acoustic bulk wave resonator consisted of a thin film of ZnO as a piezoelectric layer which has been sputtered onto a thin silicon membrane supporting structure.

The piezoelectric layer of ZnO is used to excite a longitudinal bulk wave which the wave gets reflected from the membrane and the free surface or the cavity. The authors presented a fabricated device with fundamental resonant frequencies near 500 MHz with a parallel resonant quality factor over 9000 [248]. However, these developed devices in the early stages are operating with less than one GHz resonant frequency and more investigation and development have been done to enhance the sensitivity of the FBAR device through several techniques including the optimization of the resonant frequency and electromechanical coupling coefficient which are considered the most effective method for FBAR sensitivity enhancement and quality factor improvement [119, 252–256].

Additionally, the working mechanism and operation of the FBAR are based on the same principle of the QCM devices; however, FBAR devices have some main differences such as transduction material or piezoelectric material which is sandwiched between the two metallic electrodes and its thickness and size [111, 184, 257]. The quartz crystal material that is being used in QCM has been replaced with thin film piezoelectric material in FBAR devices. Figure 12 schematically presents the cross section of the three different types of FBAR sensors, which are the SMR, air gap-based FBAR and the cavity-based FBAR which has a back-trench structure [245].

Furthermore, FBAR possesses more favored piezoelectric properties including high acoustic velocity [258], high electromechanical coupling coefficient (k^2) [259], and low acoustic loss [260]. It has been proven that bringing all these unique properties besides the ultra-thin piezoelectric films such as AlN which is in the thickness of a nanometer, all of these properties can help to produce unique FBAR devices which possess very high resonant frequencies usually from sub-GHz to 10 GHz and high-quality factor [261]. On the other hand, to reflect the acoustic wave, the FBAR active region must be totally isolated from the operational substrate; otherwise, the acoustic wave produced by the piezoelectric film would penetrate the substrate, causing the waves to be lost. As a consequence, there will be no resonance [257].

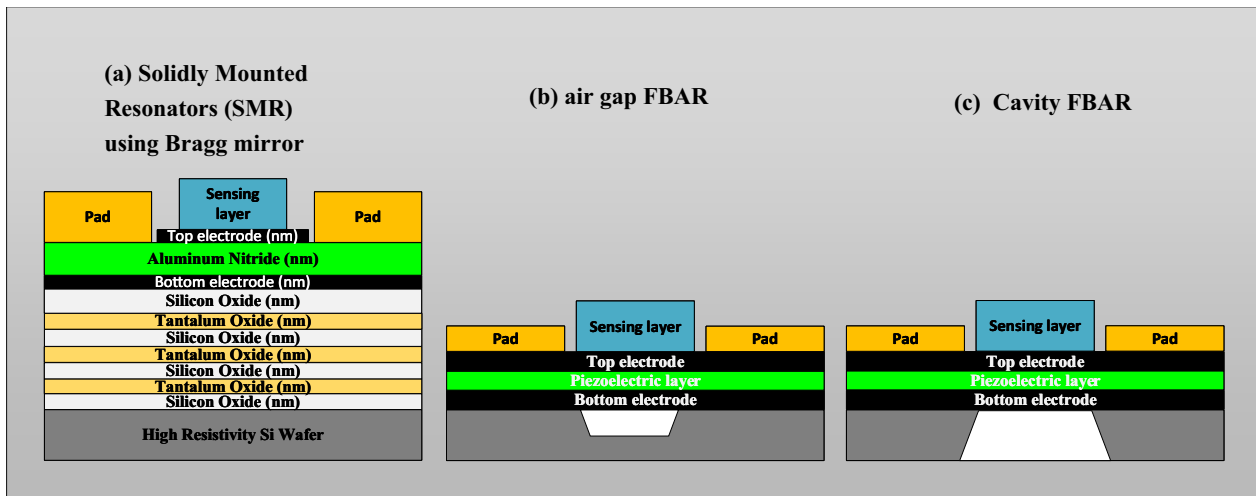


Fig. 12 Typical schematic of three different types of FBAR, **(a)** SMR based FBAR [348], **(b)** Air gap based FBAR [349], and **(c)** the Cavity based FBAR using back etch [244, 350]

Therefore, the structure of the FBAR has been developed into two different basic types of device structure. The first structure is the air-cavity resonator which can be further divided into several sub-categories depending on the etching method of the back-trench, such as the air cavity and back-trench which are either etched into or on the substrate [262, 263].

The second FBAR structure is the solidly mounted resonator (SMR) [264] which is made by separating the acoustic resonant wave by using an acoustic Bragg reflector which is consisted of several layers of certain types of materials usually called the Bragg mirror FBAR resonator [265–267]. Both the air cavity and Bragg mirror layer methods have been demonstrated to be effective reflectors and the acoustic waves have been formed between two electrodes known as metallic top and bottom electrodes.

Recently, several methods have been utilized to develop the FBAR structure. One of the various approaches to FBAR structures was created by employing certain materials such as a polymer which has very low acoustic impedance; therefore, it has shown excellent properties to be used as the acoustic reflector; therefore, the FBAR may be manufactured on any solid substrate, such as copper film or glass [268–270].

In more detail, the FBAR can be operated in two basic resonant modes: The first mode is known as the longitudinal mode, and it generates a longitudinal acoustic wave across the two surfaces of the top and bottom electrodes when an RF signal is applied to both electrodes [271–273]. The second mode is known as the thickness-shear mode, and it occurs when a shear wave is formed between the top and bottom electrodes as a response to the applied alternating voltage. The main differences between these two vibration modes are depending on the c-axis angle of the piezoelectric films. In the fabrication of the FBAR devices with shear mode, the crystal orientation of the piezoelectric material is usually off the c-axis [274], whereas the FBAR with the longitudinal mode, the piezoelectric films are usually fabricated with a crystal orientation that is normal to the film plane or substrate as shown in Fig. 13.

The performance of the FBAR with longitudinal and shear mode have been investigated experimentally in the air and liquid environment. In the liquid environment, the shear mode presented high sensitivity and quality factor because the shear waves travel in plane with little damping of resonant waves in liquid, whereas the longitudinal mode waves demonstrated excellent performance such as high sensitivity and high-quality factor in the air environment, however, less responses in the liquid environment [71, 275]. Therefore, the shear mode can work in both dry and liquid environments [115]; however, the longitudinal is only able to work outside liquid conditions. As a result, the shear mode can be utilized in the biosensor application and gas sensors, but the longitudinal mode is only suitable for gas sensors [112, 276, 277].

Furthermore, the behavior of the resonant frequency of the FBAR has been proven theoretically and experimentally in several publications. It is well known that the resonant frequency of the FBAR decreases when additional mass is added to the device's active area surface. Therefore, in the FBAR gas sensors, the gas adsorption by the sensing layer can be monitored through measuring the changes in the resonant frequency which is affected by the mass changes. Sauerbrey identified the link between increased mass and resonant frequency shift in 1959 [173] as shown in Eq. (6):

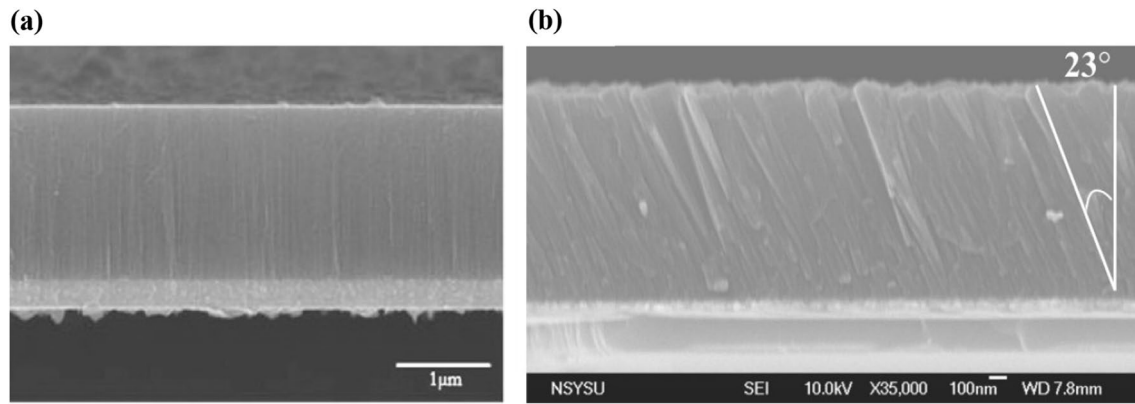


Fig. 13 SEM images of the piezoelectric thin film **(a)** cross-sectional view of AlN in the longitudinal mode, produced by [351] **(b)** cross-sectional view of AlN in the f shear mode produced by [274]

$$\Delta f = -\frac{2f_r^n}{A\sqrt{\rho_q\mu_q}}\Delta m \quad (6)$$

where Δf is the frequency change (Hz), f_r is the resonant frequency (Hz), Δm is the mass changes in the surface of the active layer (g), A is the piezoelectrically active area (cm^2), μ_q is the shear modulus of piezoelectric material ($g/cm\ s^2$), ρ_q is the density of the piezoelectric material (g/cm^3), and n is number between 1 and 2 applicable for biosensors application. Equation (6) was developed to express the relationship between the additional mass and the responses of the resonant frequency.

In addition, the Sauerbrey equation (6) is dependent on another equation which is used to calculate the frequency resonant as shown in equation (7):

$$f_r = \frac{v_s}{2h} \quad (7)$$

where h is the thickness of the piezoelectric thin film, and v_s is the acoustic velocity. Therefore, the resonant frequency is always determined and modified through the thickness of the piezoelectric material. In the FBAR sensors, the thickness of the used piezoelectric thin film is usually in the sub-micrometer to micrometer range, giving resonance frequencies varying between a few hundreds of MHz to 10 GHz and more than in some FBAR with thinner piezoelectric films in the range of nanometers [278]. According to the Sauerbrey equation, the sensitivity of the FBAR resonator is proportional to the device's resonant frequency and inversely related to the active area of the sensor. From these two parameters, the FBAR is considered more advanced compared with QCM and SAW [59, 184].

Furthermore, The FBAR quality factor is a dimensionless quantity that represents the resonator's underdamped performance and expressed the correlation between the resonator bandwidth and its center frequency [279, 280]. On other hand, the quality factor is well known and defined as the ratio of the energy stored in the resonator to the energy dissipated for each electromechanical conversion cycle [281, 282], as presented in Eq. (8):

$$Q = 2\pi \frac{\text{Energy stored}}{\text{Energy dissipated per cycle}} \quad (8)$$

where the Energy stored is represented the vibration energy stored in the resonator which is divided by the energy of the vibration that dissipated per each cycle. The device with a high-quality factor usually has less energy dissipation per each cycle. In the last few decades, researchers have been investigating the energy loss mechanism in MEMS resonators to enhance the device's performance. The most relevant loss mechanisms in the piezoelectric MEMS resonators such as the Lamé wave resonators are the loss caused by the anchor, interface between the parts loss, thermoelastic damping (TED), material damping, as well as other unknown causes of loss. It has been proven that in the Lamé wave resonators, the anchor loss is responsible for the largest proportion of the various energy losses in the MEMS resonators [283–286].

Additionally, the quality factor can also be expressed in the term of resonant frequency to the bandwidth as shown in [287]. The bandwidth is determined by taking the -3 dB points difference as expressed in Eq. (9):

$$Q = \frac{f_r}{\Delta f} \quad (9)$$

where f_r is the resonant frequency, and the Δf is the differences between the two frequencies before and after the detection processes. The FBAR sensors with a high-quality factor values are gives a more accurate reading in monitoring small frequency shifts. The FBAR with high Q usually has sharper resonant peaks compared with FBAR sensors that have lower Q values. Therefore, the sensitivity of the FBAR sensors is principally determined by both the values of resonant frequency and the quality factor.

Furthermore, the FBAR sensors are basically excited by applying a radio frequency signal on both the top and bottom electrodes of the FBAR sensor; therefore, the device performance is significantly governed by various parameters such as the temperature, piezoelectric materials properties, and electromechanical coupling coefficient (k^2) [288]. The electromechanical coupling coefficient is a measurement that is used to express what portion of the applied energy is incorporated or linked into the device [111]. The (k^2) can be calculated as expressed in Eq. (10):

$$k^2 = e_{31}^2 / (c_{11} \cdot \epsilon_{33}) \quad (10)$$

where e_{31}^2 is the electric field, the c_{11} is the elastic constant, and ϵ_{33} is the permittivity of the piezoelectric material. It is obvious that the k^2 depends on the properties of the piezoelectric material used in the device, and the electric field of the device [289]. In addition, there are several other factors that can affect the k^2 of the FBAR sensors such as the loss in the piezoelectric thin film and the electrode material, thickness, and other properties [118]. The effective electromechanical coupling coefficient k_{eff}^2 is the most common term used for the piezoelectric material assessment. The k_{eff}^2 can be evaluated by Eq. (11):

$$k_{\text{eff}}^2 = \frac{\pi^2}{4} \left(\frac{f_p - f_s}{f_p} \right); \text{ or } k_{\text{eff}}^2 = \frac{f_p^2 - f_s^2}{f_p^2} \quad (11)$$

where f_p, f_s are the parallel and series resonance frequencies, respectively. The value of this assessment for FBAR sensor is a relatively small value like other acoustic resonators, which is mostly less than 10%.

Furthermore, the quality and performance of the FBAR sensors are significantly affected by the properties and the quality of the piezoelectric thin film material. Various requirements must be considered to fabricate high-quality FBAR sensors including excellent piezoelectric properties with high electromechanical coupling coefficient k^2 , perfectly organized microstructures such as off-axis orientation with a certain angle for shear mode, easy fabrication process with low cost, etc. [71, 258].

Therefore, the selection of the piezoelectric material is crucial for the development of the FBAR sensors. Currently, there are a variety of piezoelectric materials that have been used for FBAR such as aluminum nitride (AlN), zinc oxide (ZnO), gallium arsenide (GaAs), lead zirconate (PZT), and polyvinylidene fluoride (PVDF). Each of these materials has some strengths and limitations in their properties; for instance, the AlN piezoelectric thin films have shown excellent properties such as high phase velocity, which is suitable for high resonant frequency resonator, easy fabrication process provided by MEMSCAP by PiezoMUMPs technology [245, 290, 291], as well as AlN presented strength and chemical stability, although the production procedure for AlN thin film has relatively small (k^2) value compared with ZnO.

In addition, the ZnO piezoelectric material thin film has shown good piezoelectric properties and high k^2 compared with AlN film, as well as being highly biocompatible which is believed to be excellent for bioapplications. Likewise, ZnO thin film has been used extensively in various applications during certain times; however, ZnO piezoelectric is hard to be fabricated using modern microelectronic fabrication factories such as MEMSCAP as well as it is not COMS compatible; therefore, these limitations have affected utilizing ZnO thin film in mass production and various application. Furthermore, PZT piezoelectric thin film has shown very high piezoelectric constant and (k^2) value, but it has some drawbacks such as lower wave velocity, higher acoustic wave attenuation, and some difficulties in thin film fabrication processes [11, 14, 160, 175].

Additionally, PVDF, SiC, and GaAs piezoelectric thin films have not been used extensively due to some disadvantages such as poor piezoelectric properties and high fabrication cost, and expensive material [112]. In fact, there are some other piezoelectric thin film materials that are being developed for FBAR devices such as gallium nitride (GaN) and barium strontium titanate (BST), particularly for high-frequency devices for communication applications. To culminate with the piezoelectric material that has been used for thin film fabrication for FBAR development, the AlN and ZnO have

been strongly considered the most used and useful piezoelectric materials for fabricating FBAR devices, and the choice between both is depending on the applications and fabrication tools accessibility [292–294].

Furthermore, various methods have been investigated and developed for improving the quality factor, sensitivity, and performance of the FBAR sensors including the choice and development of the piezoelectric thin film material as well as the bottom and top electrode materials, optimizing the device structures, the thickness of the piezoelectric thin film, and the fabrication processes for the FBAR. In addition to the previous explanation for the piezoelectric thin film material properties, the properties of the top and bottom electrodes material are also affecting the performance of the FBAR sensors significantly. The electrode materials must have certain properties to reflect the wave propagation such as high elastic modulus, high acoustic impedance, low mass density, high conductivity, and high acoustic impedance that mismatch with the piezoelectric thin film [295]. In particular, the material with high mass density and low acoustic impedance is not suitable for the electrodes as shown in Fig. 14 which clearly demonstrated the Density and the acoustic impedance of commonly used materials as top and bottom electrode metals. The best material would be located at the top-left corner such as the CNT, Mo, and Cr, these materials have low mass density and high acoustic impedance. Therefore, the most appropriate materials for the FBAR electrode are graphene and CNT which possess low mass density and high acoustic impedance [295]. There are still various materials with unique properties that have yet to be investigated to enhance the properties of the piezoelectric layer and electrodes [295].

Chang et al. [296] have fabricated high working frequency FBAR sensors (4.44 GHz), each individual FBAR sensor was coated with different self-assembled monolayers (SAMs) sensitive layers to establish such E-nose gas sensors. Nine different sensitive materials were used for FBAR surface functionalization, and five different VOCs target were used for the FBAR sensor characterization. The nine functionalized FBARs were tested in a glass chamber and the processes were first started by flushing the device and chamber with pure nitrogen to reach a stable baseline. The FBAR sensors successfully responded once they were exposed to VOCs gas where the sensor resonant frequency decreased due to the gas molecule adsorption reaction. Furthermore, the FBAR sensor showed resonant frequency increasing due to the molecule desorption processes due to the replacement of the VOCs gases with nitrogen. Thus, the FBAR sensors with different SAMs have clearly demonstrated that the adsorption–desorption process is a completely reversible process, which is depending on the monolayer surface modifications. The reversibility process is an extremely important feature in the E-nose and gas sensors application since incomplete desorption will give an unreasonable reading and the sensor will be malfunctioning. The authors investigated and presented the effects of the functional group's properties on the gas–surface interactions.

Chen et al. [297] have fabricated FBAR and developed a promising strategy to combine the benefits of a microelectromechanical system and the nanostructure of nanofibers for the detection of gases in low concentration. The developed FBARs are working at 4.4 GHz which is performing as a sensitive mass loading platform. Polyethyleneimine nanofibers were prepared and directly deposited by the electrospinning method on the FBAR surface. The adsorption and diffusion of the formaldehyde gas were investigated and the three-dimensional structure of the polyethyleneimine nanofibers presented a large surface area for the detection processes. The resonant frequency of the FBAR presented a downshift due to the ultra-small mass change induced by the formaldehyde molecules' adsorption onto the amine groups that were provided by the polyethyleneimine surface. The fabricated FBAR sensors demonstrated high sensitivity, excellent selectivity, good reversibility, fast and linear response toward formaldehyde molecules. The sensitivity and detection limit were obtained to be 1.216 kHz/ ppb and 37 ppb, respectively.

Wang et al. [298] have developed a microscale AlN-based film bulk acoustic resonator for formaldehyde vapor detection based on a mass-sensitive mechanism. The authors implement layer-by-layer sensitive coating techniques

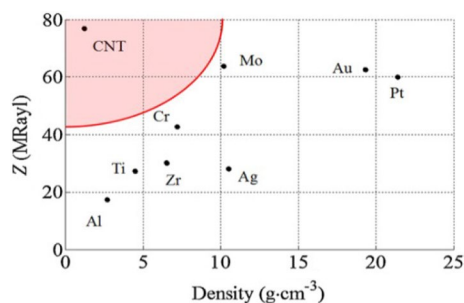


Fig. 14 Density and acoustic impedance of commonly used electrode metals, produced by [295]

on the resonator surface utilizing single and multi-walled carbon nanotubes/polyethyleneimine multilayers. The FBAR sensor response was observed after several nanotubes/polyethyleneimine layers were deposited on the surface of the FBAR with an almost linear decrease in the resonant frequency. The reduction in the resonant frequency has approved the mechanism of the mass sensing techniques. Furthermore, the FBAR sensor showed a linear relationship between the concentration of the formaldehyde and the resonant frequency shift. The developed sensitive layer presented a random and porous structure and provided a large surface area which provided enough vacancies for gas adsorption, on the other hand, the FBAR sensor demonstrated excellent selectivity toward the formaldehyde gas molecules thanks to the strong affinity provided by the amine groups in the polyethyleneimine layer, thus the selectivity is always depended on the properties and the modification of the sensitive layer such as surface area, quantity, and quality of the amine or other functional groups that generated by the surface functionalization processes [91]. The authors also demonstrated that the number of the sensitive layers had extremely influenced the adsorption behavior and detection processes. The developed FBAR gas sensor works at an ultra-high resonant frequency of 4.8 GHz and shows good sensitivity in the range of 1.29–1.90 kHz ppb⁻¹ and a limit of detection between 24 and 38 ppb [298]. Furthermore, the authors investigated the influence and the effects of the spraying processes on the sensor performance for formaldehyde detection processes. The sensor response and the reaction between the amine functional groups on the polyethyleneimine surface and the target gas were presented and investigated [299].

Furthermore, Song et al. [300] have also utilized self-assembled polyethyleneimine-modified with single-wall carbon nanotubes as a sensitive coating material in the FBAR for formaldehyde gas detection at room temperature. The fabricated FBAR sensor has been fabricated using 1 μm AlN piezoelectric thin film which provided ultra-high resonant frequency (4.5 GHz). The FBAR has demonstrated the ability to detect small mass changes in the sensitive layer on the top surface of the device which is induced by the adsorption of the target gas molecules. The reversibility and selectivity have been demonstrated by the proposed FBAR sensor. Furthermore, the sensitivity and frequency response of the sensor were significantly improved by increasing the area covered by the carbon nanotubes on the sensor surface due to the excellent properties of the carbon nanotubes such as large surface area, and good adsorption properties. The fabricated FBAR sensor has been tested for formaldehyde molecules detection and the sensor presented a linear response toward the targeted gas in the range of 50–400 ppb with a 24 ppb limit of detection. Therefore, these results prove that the FBAR sensor is a promising device to be used for portable and convenient detection of indoor air pollution at room temperature.

Furthermore, Jilong Ma et al. [301] developed another type of FBAR using a ZnO piezoelectric thin film layer instead of AlN. The prepared FBAR sensors have been used for formaldehyde gas detection. Multi-walled carbon nanotubes/polyethyleneimine bilayer was developed as a sensitive layer for the detection processes and was self-assembled on the resonator surface. The fabricated FBAR sensors have been developed using the Bragg reflector technique through SiO_2/W layers. The sensitivity and selectivity of the FBAR sensors toward formaldehyde molecules have been enhanced by the amine functional groups on the polyethyleneimine. The authors presented a reversible nucleophilic addition reaction between the formaldehyde gas molecules and the amine functional groups that available on the polyethyleneimine surface; thus, the multi-walled carbon nanotubes/polyethyleneimine sensitive layer demonstrated excellent adsorption toward the formaldehyde gas. Additionally, the developed FBAR sensor with a high working frequency of 3.1 GHz has presented high and excellent mass sensitivity and ultra-small mass change detection with a linear relationship between the increase in the formaldehyde gas concentration and the resonant frequency downshift. This FBAR sensor has shown excellent results for formaldehyde gas concentration in the range of 50–400 ppb at room temperature.

In addition, Zeng et al. [302] have developed single film bulk acoustic wave resonator for the detection and discrimination of volatile organic compounds (VOCs) utilizing highly sensitive coated material which consisted of 20-bilayer self-assembled poly (sodium 4-styrene sulfonate)/poly (diallyl dimethyl ammonium chloride) thin film. The authors have conducted proof-of-concept validation processes for the fabricated FBAR by exposing the device to six different VOC vapors at six different gas partial pressures. The device was successfully detecting the target gases in real time with static and dynamic detection. The FBAR frequency shifts and impedance responses were measured and evaluated using several analysis techniques, which present that all types of exposed gases can be detected, classified, and distinguished with an

accuracy of more than 97%. The FBAR sensor has been designed to be working with a resonant frequency of 2.45 GHz which provides excellent sensitivity and a low limit of detection. This research investigated the effects of temperature modulation on the adsorption and desorption of different VOCs. Furthermore, the authors presented the capability of the FBAR sensor to discriminate different VOCs by using measuring the frequencies and impedance responses under different temperatures. This type of FBAR gas sensor demonstrated simple mass-based electronic detection tools with ultrasensitive capability, low cost, small size, and stable working temperature with minimizing the affecting of ambient temperature fluctuation. These unique features give the FBAR potential to be used and integrated into small electronic circuits such as mobile phones.

Liu et al. [280] have developed a high-performance film acoustic resonator for humidity mentoring. The published paper presented the design, simulation, fabrication, and characterization of the FBAR sensor for humidity detection. Polyimide film was employed to be used as a humidity-sensing layer and to provide structural support for the device. The FBAR sensor was tested with and without the polyimide film and it has shown that the sensor with thin film coating has 39 times higher response than the sensor without any sensing layer, where the sensitivity reaches + 67.3 kHz/RH between 15%RH and 85%RH. The fabricated FBAR sensor was fixed on a printed circuit board (PCB) and bonded using gold wire. The S-parameters of the FBAR sensor has been measured and characterized using a network analyzer. Furthermore, all the characterization processes for the humidity response measurement were carried out using a humidity generator (MODEL 2000) in the range from 15%RH to 85%RH at room 25 °C. However, the FBAR humidity sensor is always sensitive to the temperature; therefore, the effects of the temperature on the sensor response have been characterized in the range of -50°C to +50 °C using another chamber called a high-low temperature alternating test chamber.

In addition, Yan et al. [303, 304] have utilized metal-organic frameworks (MOFs) sensitive material with high surface area (HKUST-1) in film bulk acoustic resonators to enhance the device performance. Since the sensor parameters such as sensitivity, selectivity, and the stability are mainly dependent on the properties of the prepared nanomaterials, the authors investigated various hybrids between organic and inorganic which significantly enhanced the sensor's performance. The fabricated FBAR sensor has a working resonant frequency of around 2.4 GHz and it has been used to detect several types of VOCs and water molecules. The sorptive MOF thin film was prepared through a layer-by-layer strategy.

Zhang et al. [305] have designed and fabricated FBAR gas sensors for relative humidity (RH) and ethanol detection. The fabricated FBAR was driven by a Colpitts oscillator which provides and supplies a frequency signal for the detection application. The device is fabricated from a multilayer structure, consisting of two electrodes sandwiching the ZnO piezoelectric layer. In this FBAR sensor, the ZnO has been used as piezoelectric material and sensitive layer due to the unique properties of the ZnO such as the strong physical adsorption and sensitive chemical adsorption between the crystalline ZnO and various chemicals such as ethanol, hydrogen, ozone, and water. The authors have introduced new micro through holes with a size of $10 \mu\text{m} * 10 \mu\text{m}$ within the top electrode to enlarge the reaction between the ZnO and the targeted gas molecules which will enhance the FBAR sensitivity. The effects of the micro through holes have been demonstrated experimentally where the sensitivity has been enhanced by around 3.2 times higher compared to the FBAR sensor which has a full solid top electrode. Additionally, Agilent Network Analyzer was used to determine the sensor impedance characteristics, In addition, a CXA signal analyzer and a mixed signal oscilloscope were utilized to identify the sensor's output signals. A Moisture Generator regulated the temperature and humidity, and the detection was conducted in a static condition. The sensor was operated with a voltage supply of 3 V and the sensor's output signal was detected at a power of -2.6 dBm and phase noise -90 dBc/Hz@ 100kHz. The sensor was used for humidity detection in the range from 25 to 88% at room temperature and the resonant frequency shift was 733 kHz.

In addition, the utilization of FBAR as a gas sensor has attracted researchers, and they still investigating the feasibility of the FBAR being used as a portable gas sensor for indoor applications. Hoffmann et al. [306] have fabricated solidly mounted FBAR with ZnO (900 nm) piezoelectric material and a working resonant frequency of around 800 MHz for humidity and carbon dioxide detection at room temperature. Since the FBAR resonant frequency is mainly dependent on the piezoelectric material thickness and acoustic velocity, the ZnO piezoelectric material has less acoustic velocity

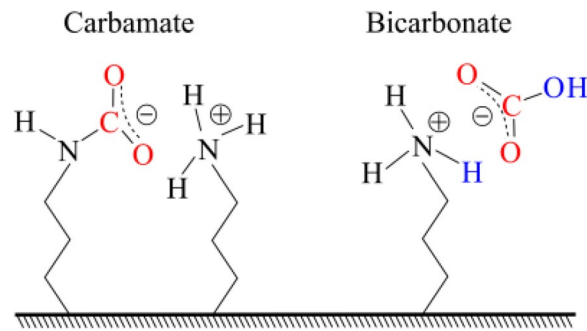


Fig. 15 The two most common interactions of CO_2 with amines, where the carbamate needs two amine groups in the vicinity, whereas bicarbonate utilizes water as a free base [306]

compared with the AIN materials; therefore, the resonant frequency in this FBAR is less than 1 GHz. The authors investigated two different sensitive materials including polyaminosiloxane and ethyl cellulose to be used for FBAR surface functionalization. The FBAR response for CO_2 has been demonstrated with a resolution of 50 ppm in the range of 400 and 1000 ppm. The density of the adsorption layer and the acoustic velocity of the device have been expressed by using the Mason model and the correlation between the changes in these parameters and the effect in the resonant frequency has been highlighted.

Furthermore, the FBAR has been coated with functional groups for CO_2 detection, in fact, there are various types of functional groups that have been used for CO_2 adsorption as summarized by Choi et al. [307]. However, amine-based organic compounds are considered one of the most promising sensitive layers for CO_2 detection application. It has been known that amines can bind with carbon dioxide through acid-based reactions. Furthermore, the reaction between the carbon dioxide and the amine is also depended on the atmosphere such as in an anhydrous atmosphere, there must be two moles of amine for one mole of CO_2 to bind in the form of carbamate as shown in Fig. 15 in addition, in hydrous atmosphere, water molecules can act as an additional free base, thus only one amine group is necessary to be bound with CO_2 , and this reaction will form bicarbonate species [307–313].

Furthermore, the film bulk acoustic resonator has attracted researchers' attention for its promising features, especially in high-frequency applications. The traditional radio frequency filters cannot meet the demands of high-frequency application, integration, and miniaturization features. Therefore, there is a new horizon that appears for FBAR in the high-frequency application. Additionally, there are some scholars extensively investigating the capability of the FBAR for several applications such as communication filters [314–318] and chemical detection [257, 319–321].

In addition, the researchers are still investigating the FBAR parameters for enhancing the device performance such as the quality factor, coupling coefficient, electromechanical coupling, device geometry, and the figure of merit [261, 268, 288, 322–326]. For instance, Johar et al. [327] have optimized FBAR for toluene gas detection. The authors reported an optimized design of a flexible film bulk acoustic resonator with polyethylene terephthalate as a flexible substrate. Furthermore, the paper investigated the performance of different piezoelectric materials such as aluminum nitride, zinc oxide, and zirconate titanate with a polydimethylsiloxane (PDMS) sensitive layer coated on the top electrode for toluene gas detection. Furthermore, the Bragg reflector stages and the effect of the PDMS layer thickness on the performance of the sensor were presented using finite element modeling and the optimal configuration was obtained using Taguchi DoE and ANOVA techniques. The results for the optimized structure have been presented for the coupling coefficient, quality factor, and figure of merit which are 23.7874%, 991, and 235, respectively. Table 5 summarizes the related FBAR sensors that have been developed for gas detection applications.

Table 5 Summary of related FBAR sensors for gas detection

Piezoelectric materials	Device frequency (MHz)	Sensing layer	Target	Limit of detection	Frequency shift	Temp	Year	Ref
AlN	4.8 GHz	CNT/polyethyl-eneimine	Formaldehyde	24–38 ppb	1.29–1.9 kHz/ppb	RT	2018	[298]
AlN	4.5 GHz	SWCNT/polyethyl-eneimine	Formaldehyde	82–143 ppb	0.412–0.301 kHz/ppb	RT	2018	[300]
AlN	4.44 GHz	Nine-SAM	VOCs	N/G	n/g	RT	2016	[296]
AlN	4.4 GHz	Polyethyleneimine nanofibers	Formaldehyde	37 ppb.	1.216 kHz/ppb	RT	2018	[297]
ZnO	3.1 GHz	MWCNT/polyethyl-eneimine	Formaldehyde	50–400 ppb	1.4–2.13 kHz/ppb	RT	2018	[301]
AlN	2.45 GHz	Hybrid thin film	VOCs	40–180 ppb	0.05 kHz/ppm	RT	2019	[302]
AlN	2.4 GHz	MOFs	VOCs	1 ppm	0.28–1.27 kHz/ppm	RT	2020	[303, 304]
ZnO	1.15 GHz	Polyimide	Humidity	15–85%	67.3 kHz/%RH	RT	2020	[280]
ZnO	800 MHz	Ethyl cellulose, poly-siloxanes	CO ₂	50 ppm	N/G	RT	2017	[306]
ZnO	N/G GHz	ZnO	Humidity, ethanol	25–88%	733 kHz/%RH	RT	2017	[305]

N/G Not given

Table 6 Summary of common piezoelectric-based sensors for gases detection

Device type	Piezoelectric material	Device frequency (GHz)	Sensing material	Targeted gas	LOD (ppm)	Frequency shift (Hz/ppm)	Response time (S)	Recovery time (S)	Temp	Year	Refs
QCM	AT-CUT	0.005	Polymer/GNR	NH ₃	70	106	1800	n/g	RT	2021	[169]
QCM	AT-CUT	0.009	ZIF	CO ₂	n/g	n/g	n/g	n/g	RT	2018	[333]
QCM	AT-CUT	0.009	(ZIF-8)	CO ₂	10,00,000	217	10	n/g	RT	2018	[215]
QCM	AT-CUT	0.01	rGO	CO ₂	50–500	50	26	10	RT	2021	[176]
QCM	AT-CUT	0.01	MOF	CO ₂	400–500	n/g	n/g	n/g	RT	2018	[179]
QCM	AT-CUT	0.025	PAAM/MWCNTs	Formaldehyde	0.5	3	80	100	RT	2021	[331]
SAW	ST-cut quartz	0.2	SiO ₂ , TiO ₂	NO ₂	16	112 KHz/40ppm	80	50	RT	2017	[218]
SAW	ST-cut quartz	0.4341	Nickel–Graphene	CO ₂	200	2.07	–	–	RT	2015	[336]
SAW	ST-cut quartz	0.2	GO Nanofilm	CH ₃	500	620 Hz/500ppb	100	500	RT	2019	[338]
SAW	ST-cut quartz	0.2	Boehmite.	NH ₃	10	1540 Hz/10ppm	n/g	n/g	RT	2019	[341]
SAW	Y-Z LiNbO ₃	0.436	ZIF-8	CO ₂	0.38	1.396 rad	n/g	n/g	RT	2018	[215]
SAW	Y-Z LiNbO ₃	0.86	ZIF-8	CO ₂	0.91	1.11 rad	n/g	n/g	RT	2020	[216]
FBAR	ZnO	0.8	Ethyl cellulose	CO ₂	50 ppm	n/g	n/g	n/g	RT	2017	[306]
FBAR	AlN	2.4	MOFs	VOCs	1 ppm	0.28–1.27 KHz/ppm	n/g	n/g	RT	2020	[303, 304]
FBAR	AlN	2.45	Hybrid thin film	VOCs	40–180 ppb	0.05 KHz/ppm	n/g	n/g	RT	2019	[302]
FBAR	ZnO	3.1	MWCNT -hybrid	Formaldehyde	50–400 ppb	1.4–2.13 KHz/ppb	–	–	RT	2018	[301]
FBAR	AlN	4.4	polyethyleneimine nanofibers	Formaldehyde	37	1.216 KHz/ppb	25	60	RT	2018	[297]
FBAR	AlN	4.8	“Polyethyleneimine /CNT”	Formaldehyde	24–38 ppb	1.29–1.9 KHz/ppb	57	59	RT	2018	[298]

n/g = not given

Summary of common piezoelectric-based sensors for gas detection

The piezoelectric-based gas sensors have been summarized in this section as presented in Table 6. The piezoelectric sensors that work based on the QCM technology usually have less resonant frequency compared with the FBAR sensors; therefore, the QCM sensors are not provided highly sensitive features and its bulk quartz layer is not compatible with CMOS fabrication technology. As a result, the QCM is not supporting the future trends of sensors integration and monolithic approaches. Furthermore, the piezoelectric gas sensors based on the SAW technology have a working resonant frequency of less than 1 GHz, and the acoustic wave is propagating on the surface of the device compared with the FBAR in which the acoustic wave is propagating inside the bulk piezoelectric layer; therefore, the SAW sensors are provided low sensitivity compared with the FBAR sensor. In addition, from the literature, the PMUT sensors are mainly used for medical imaging and in fingerprint application rather than the gas sensor application. Therefore, the FBAR technology seems to provide a unique platform for gas sensing applications, especially since it has the feasibility to be fabricated with CMOS fabrication compatibility and monolithically.

Summary

The present work reviewed the scientific literature that addressed the piezoelectric-based MEMS gas sensors, starting from the historical background of the piezoelectric sensors and including the development of each piezoelectric device, their design and simulation, experiments, and sensing capabilities. Several piezoelectric transducers have experimented for detecting small trace gas molecules. The most commonly developed piezoelectric-based MEMS have been investigated in detail, such as the piezoelectric microcantilever, surface acoustic wave, quartz crystal microbalance, piezoelectric micromachined ultrasonic transducer, and the film bulk acoustic wave resonators. In particular, the papers that quantitatively demonstrated the capability of the piezoelectric devices through simulation, fabrication, and verification have been analyzed comprehensively. Overall, these piezoelectric-based MEMS sensors demonstrated unique properties to be used as gas sensors which have the capability of detecting trace gas molecules and have the feasibility to be fabricated with CMOS technology to be built-in sensors.

Acknowledgements This work was supported by Universiti Teknologi PETRONAS under Yayasan Universiti Teknologi PETRONAS (YUTP) Grant number 015LCO-181. The authors would like to thank the department of Electrical and Electronic Engineering as well as the Centre of Graduate Studies (CGS) in Universiti Teknologi PETRONAS (UTP) for providing the research facilities and funding this research.

Author contributions SSBH, MHMK, and YA-D contributed to conceptualization; SSBH, MHMK, UIB, IMN, YA-D, OLA-M, FZ, and MGJ contributed to methodology; SSBH, MHMK, YA-D, UIB, FZ, MOBS, MG Junaid, MH, and SSA investigated the study; SSBH, MHMK, UIB, FZ, and ASA provided resources; SSBH, MHMK, UIB, ASA, and SSA curated the data; SSBH and MHMK contributed to writing—original draft preparation; SSBH, MHMK, YA-D, FZ, and UIB contributed to writing—review and editing; SSBH, UIB, and ASA visualized the study; MHMK, YA-D, and IMN supervised the study; SSBH, MHMK, IMN, ASA, and FZ administered the project; MHMK, SSBH, and FZ performed funding acquisition. All authors have read and agreed to the published version of the manuscript.

Funding This research was funded by the Yayasan Universiti Teknologi PETRONAS (YUTP) Fundamental Research Grant with cost center 015LCO-181.

Data availability The data reported in this research are available from the corresponding author upon request.

Declaration

Ethics approval and consent to participate The authors agree to participate.

Consent for publication The authors agree to publish this manuscript.

Competing interests The authors declare no competing interests.

Open Access This article is licensed under a Creative Commons Attribution 4.0 International License, which permits use, sharing, adaptation, distribution and reproduction in any medium or format, as long as you give appropriate credit to the original author(s) and the source, provide a link to the Creative Commons licence, and indicate if changes were made. The images or other third party material in this article are included in the article's Creative Commons licence, unless indicated otherwise in a credit line to the material. If material is not included in the article's Creative Commons licence and your intended use is not permitted by statutory regulation or exceeds the permitted use, you will need to obtain permission directly from the copyright holder. To view a copy of this licence, visit <http://creativecommons.org/licenses/by/4.0/>.

References

1. Fujita H. A decade of mems and its future. In: Proceedings IEEE The Tenth Annual International Workshop on Micro Electro Mechanical Systems. An Investigation of Micro Structures, Sensors, Actuators, Machines and Robots, 1997:pp. 1–7. IEEE
2. Qu H. Cmos mems fabrication technologies and devices. *Micromachines*. 2016;7(1):14.
3. Song P, Ma Z, Ma J, Yang L, Wei J, Zhao Y, Zhang M, Yang F, Wang X. Recent progress of miniature mems pressure sensors. *Micromachines*. 2020;11(1):56.
4. Verma G, Mondal K, Gupta A. Si-based mems resonant sensor: a review from microfabrication perspective. *Microelectron J*. 2021;118:105210.
5. Ikumapayi O, Akinlabi E, Adeoye A, Fatoba S. Microfabrication and nanotechnology in manufacturing system-an overview. *Mater Today: Proc*. 2021;44:1154–62.
6. Uranga A, Verd J, Barniol N. Cmos-mems resonators: from devices to applications. *Microelectron Eng*. 2015;132:58–73.
7. Fedder GK, Howe RT, Liu TJK, Quevy EP. Technologies for cofabricating mems and electronics. *Proc IEEE*. 2008;96(2):306–22.
8. Khaniki HB, Ghayesh MH, Amabili M. A review on the statics and dynamics of electrically actuated nano and micro structures. *Int J Non-Linear Mech*. 2021;129:103658.
9. Algamil AS, Khir MHM, Dennis JO, Ahmed AY, Alabsi SS, Ba Hashwan SS, Junaid MM. A review of actuation and sensing mechanisms in mems-based sensor devices. *Nanoscale Res Lett*. 2021;16(1):1–21.
10. Nguyen PH, Zhang W. Design and computational modeling of fabric soft pneumatic actuators for wearable assistive devices. *Sci Rep*. 2020;10(1):1–13.
11. Ali WR, Prasad M. Piezoelectric mems based acoustic sensors: a review. *Sens Actuators A*. 2020;301:111756.
12. Ashraf MW, Tayyaba S, Afzulpurkar N. Micro electromechanical systems (mems) based microfluidic devices for biomedical applications. *Int J Mol Sci*. 2011;12(6):3648–704.
13. Ceyssens F, Sadeghpour S, Fujita H, Puers R. Actuators: accomplishments, opportunities and challenges. *Sens Actuators A*. 2019;295:604–11.
14. Chorsi MT, Curry EJ, Chorsi HT, Das R, Baroody J, Purohit PK, Ilies H, Nguyen TD. Piezoelectric biomaterials for sensors and actuators. *Adv Mater*. 2019;31(1):1802084.
15. Rupitsch SJ. Piezoelectric sensors and actuators. Simulation of Piezoelectric Sensor and Actuator Devices. In: *Piezoelectric Sensors and Actuators. Topics in Mining, Metallurgy and Materials Engineering*, 2019:83–126
16. Zawawi SA, Hamzah AA, Majlis BY, Mohd-Yasin F. A review of mems capacitive microphones. *Micromachines*. 2020;11(5):484.
17. Smith CS. Piezoresistance effect in germanium and silicon. *Phys Rev*. 1954;94(1):42.
18. Muro H. History and recent progress of mems physical sensors. *Adv Sci Technol*. 2013;81:1–8.
19. Feynman RP. There's plenty of room at the bottom [data storage]. *J Microelectromech Syst*. 1992;1(1):60–6.

20. Feynman R. There's plenty of room at the bottom. In: Feynman and Computation, CRC Press, 2018:pp. 63–76.
21. Colaço R, Serro AP. Nanoscale wear of hard materials: an overview. *Curr Opin Colloid Interface Sci.* 2020;47:118–25.
22. Manrique-Juarez MD, Rat S, Salmon L, Molnár G, Quintero CM, Nicu L, Shepherd HJ, Bousseksou A. Switchable molecule-based materials for micro-and nanoscale actuating applications: achievements and prospects. *Coord Chem Rev.* 2016;308:395–408.
23. Zang X, Zhou Q, Chang J, Liu Y, Lin L. Graphene and carbon nanotube (cnt) in mems/nems applications. *Microelectron Eng.* 2015;132:192–206.
24. Ando T, Fu X-A. Materials: silicon and beyond. *Sens Actuators A.* 2019;296:340–51.
25. Lee HJ, Choi N, Yoon E-S, Cho I-J. MemS devices for drug delivery. *Adv Drug Deliv Rev.* 2018;128:132–47.
26. Ejeian F, Azadi S, Razmjou A, Orooji Y, Kottapalli A, Warkiani ME, Asadnia M. Design and applications of mems flow sensors: a review. *Sens Actuators A.* 2019;295:483–502.
27. Forouzanfar S, Pala N, Madou M, Wang C. Perspectives on c-mems and c-nems biotech applications. *Biosens Bioelectron.* 2021;180:113119.
28. Bogue R. Recent developments in mems sensors: a review of applications, markets and technologies. *Sensor Rev.* 2013.
29. Mishra MK, Dubey V, Mishra P, Khan I. MemS technology: a review. *J Eng Res Rep.* 2019;4(1):1–24.
30. Hajare R, Reddy V, Srikanth R. MemS based sensors—a comprehensive review of commonly used fabrication techniques. *Mater Today: Proc.* 2021.
31. Cao Y, Wang P, Li J, Xie H. Temperature stability study of resonant angular scanning micromirrors with electrostatic comb-drive actuators. *Sens Actuators A.* 2021;318: 112525.
32. Jiang B, Peng M, Liu Y, Zhou T, Su Y. The fabrication of 2d micromirror with large electromagnetic driving forces. *Sens Actuators A.* 2019;286:163–8.
33. Moallemi A, Fan R, Zhang Y, Foroughi AF, Chen L, Zhao Y, Wu Z, Nagamune R, Chou KC, Zeng H, et al. Development of a hybrid piezoelectric and pneumatic miniature optical scanner for endoscopic applications. *Sens Actuators A.* 2020;315: 112311.
34. Pillai G, Li S-S. Piezoelectric memS resonators: a review. *IEEE Sens J.* 2020;21(11):12589–605.
35. Saqib M, Mubasher Saleem M, Mazhar N, Awan SU, Shahbaz Khan U. Design and analysis of a high-gain and robust multi-dof electro-thermally actuated memS gyroscope. *Micromachines.* 2018;9(11):577.
36. Cauchi M, Grech I, Mallia B, Mollicone P, Sammut N. Analytical, numerical and experimental study of a horizontal electrothermal memS microgripper for the deformability characterisation of human red blood cells. *Micromachines.* 2018;9(3):108.
37. Bukhari SAR, Saleem MM, Khan US, Hamza A, Iqbal J, Shakoor RI. Microfabrication process-driven design, fem analysis and system modeling of 3-dof drive mode and 2-dof sense mode thermally stable non-resonant memS gyroscope. *Micromachines.* 2020;11(9):862.
38. Elsayed MY, Cicek P-V, Nabki F, El-Gamal MN. Bulk mode disk resonator with transverse piezoelectric actuation and electrostatic tuning. *J Microelectromech Syst.* 2016;25(2):252–61.
39. Marigo E, Azuan MN, Amiera A, Annie L, Shazwani N, Fei CB, Soundara-Pandian M. Manufacturability of highly densed arrays of sc 20% doped aln monolithic pmut. In: 2021 IEEE 34th International Conference on Micro Electro Mechanical Systems (MEMS), 2021:1048–1050. IEEE
40. Tan TH, Soundara-Pandian M, Shazwani N, Marigo E, Raj RA, Subramaniam M. Evaluating film assisted molding packaging for peizoelectric micromachined ultrasonic transducers. In: 2021 IEEE 34th International Conference on Micro Electro Mechanical Systems (MEMS), 2021:pp. 1044–1047 . IEEE
41. Specht JP, Esfahani S, Xing Y, Köck A, Cole M, Gardner JW. Thermally modulated cmos-compatible particle sensor for air quality monitoring. *IEEE Trans Instrum Meas.* 2022;71:1–13.
42. Dehé A, Wurzer M, Földner M, Krumbein U. A4. 3-the infineon silicon memS microphone. *Proc Sensor.* 2013;2013:95–9.
43. Gourlat G, Sansa M, Villard P, Picard G, Jourdan G, Ouerghi I, Billiot G, Hentz S. 15.6 a 30-to-80mhz simultaneous dual-mode heterodyne oscillator targeting nems array gravimetric sensing applications with a 300zg mass resolution. In: 2017 IEEE International Solid-State Circuits Conference (ISSCC), 2017:pp. 266–267. IEEE
44. Sage E, Sansa M, Fostner S, Defoort M, Gély M, Naik AK, Morel R, Duraffourg L, Roukes ML, Alava T, et al. Single-particle mass spectrometry with arrays of frequency-addressed nanomechanical resonators. *Nat Commun.* 2018;9(1):1–8.
45. Karlen S, Haesler J, Overstolz T, Bergonzi G, Lecomte S. Sealing of memS atomic vapor cells using Cu–Cu thermocompression bonding. *J Microelectromech Syst.* 2019;29(1):95–9.
46. Liu C, Chou BC, Tsai RCF, Shen NY, Chen BS, Cheng EC, Tuan HC, Kalnitsky A, Cheng S, Lin CH, et al. MemS technology development and manufacturing in a cmos foundry. In: 2011 16th International Solid-State Sensors, Actuators and Microsystems Conference, 2011:pp. 807–810 . IEEE
47. Sung W, Lee F, Cheng C, Chang C, Cheng E, Fang W. MemS above cmos process for single proof-mass 3-axis lorentz-force resonant magnetic sensor. In: 2016 IEEE 29th International Conference on Micro Electro Mechanical Systems (MEMS), 2016:pp. 978–981. IEEE
48. Schwarz M, Franz J, Reimann M. The future is memS design considerations of microelectromechanical systems at bosch. In: 2015 22nd International Conference Mixed Design of Integrated Circuits & Systems (MIXDES), 2015:pp. 177–180 . IEEE
49. Hald A, Herzogenrath P, Scheible J, Lienig J, Seelhorst J, Brandl P. Full custom memS design: A new method for the analysis of motion-dependent parasitics. *Integration.* 2018;63:362–72.
50. Gerdroodbary MB, Ganji D, Shiryanpour I, Moradi R. Mass analysis of ch4/so2 gas mixture by low-pressure memS gas sensor. *J Natl Gas Sci Eng.* 2018;53:317–28.
51. Vincent TA, Gardner J. A low cost memS based ndir system for the monitoring of carbon dioxide in breath analysis at ppm levels. *Sens Actuators B Chem.* 2016;236:954–64.
52. Tabassum R, Pavelyev V, Moskalenko A, Tukmakov K, Islam S, Mishra P. A highly sensitive nitrogen dioxide gas sensor using horizontally aligned swcnts employing memS and dielectrophoresis methods. *IEEE Sensors Lett.* 2017;2(1):1–4.
53. Hagleitner C, Lange D, Hierlemann A, Brand O, Baltes H. Cmos single-chip gas detection system comprising capacitive, calorimetric and mass-sensitive microsensors. *IEEE J Solid-State Circuits.* 2002;37(12):1867–78.
54. Xu J, Setiono A, Peiner E. Piezoresistive microcantilever with sam-modified zno-nanorods@ silicon-nanopillars for room-temperature parts-per-billion NO₂ detection. *ACS Appl Nano Mater.* 2020;3(7):6609–20.

55. Toda M, Moorthi K, Hokama T, Wang Z, Yamazaki M, Ono T. Miniature piezoresistive sensor for detecting volatile organic components. *Sens Actuators B Chem.* 2021;333: 129524.
56. Ma Y, He Y, Patimisco P, Sampaolo A, Qiao S, Yu X, Tittel FK, Spagnolo V. Ultra-high sensitive trace gas detection based on light-induced thermoelastic spectroscopy and a custom quartz tuning fork. *Appl Phys Lett.* 2020;116(1): 011103.
57. Zhu Q. Microcantilever sensors in biological and chemical detections. *Sensors Trans.* 2011;125(2):1.
58. Liu Z, Chen J, Zou X. Modeling the piezoelectric cantilever resonator with different width layers. *Sensors.* 2020;21(1):87.
59. McGinn CK, Lampot ZA, Kymissis I. Review of gravimetric sensing of volatile organic compounds. *ACS Sensors.* 2020;5(6):1514–34.
60. Alexandre M, Nakamoto T. Study of room temperature ionic liquids as gas sensing materials in quartz crystal microbalances. *Sensors.* 2020;20(14):4026.
61. Johar AK, Sharma G, Kumar A, Kumar H, Varma T, Periasamy C, Agarwal A, Boolchandani D. Modeling, fabrication, and structural characterization of thin film ZnO based film bulk acoustic resonator. *Mater Today: Proc.* 2021;46:5716–21.
62. Nazemi H, Joseph A, Park J, Emadi A. Advanced micro-and nano-gas sensor technology: a review. *Sensors.* 2019;19(6):1285.
63. Lei G, Lou C, Liu X, Xie J, Li Z, Zheng W, Zhang J. Thin films of tungsten oxide materials for advanced gas sensors. *Sens Actuators B Chem.* 2021;341: 129996.
64. Drmash Q, Yamani Z, Mohamedkhair A, Hendi A, Hossain M, Ibrahim A. Gold nanoparticles incorporated SnO₂ thin film: highly responsive and selective detection of NO₂ at room temperature. *Mater Lett.* 2018;214:283–6.
65. Chinh ND, Hien TT, Van Do L, Hieu NM, Quang ND, Lee S-M, Kim C, Kim D. Adsorption/desorption kinetics of nitric oxide on zinc oxide nano film sensor enhanced by light irradiation and gold-nanoparticles decoration. *Sens Actuators B Chem.* 2019;281:262–72.
66. Zhang S, Wang J, Torad NL, Xia W, Aslam MA, Kaneti YV, Hou Z, Ding Z, Da B, Fatehmulla A, et al. Rational design of nanoporous mos2/ vs2 heteroarchitecture for ultrahigh performance ammonia sensors. *Small.* 2020;16(12):1901718.
67. Witjaksono G, Junaid M, Khir MH, Ullah Z, Tansu N, Saheed MSBM, Siddiqui MA, Ba-Hashwan SS, Algamil AS, Magsi SA, et al. Effect of nitrogen doping on the optical bandgap and electrical conductivity of nitrogen-doped reduced graphene oxide. *Molecules.* 2021;26(21):6424.
68. Jaber N, Ilyas S, Shekhah O, Eddaoudi M, Younis MI. Multimode excitation of a metal organics frameworks coated microbeam for smart gas sensing and actuation. *Sens Actuators A.* 2018;283:254–62.
69. Vidana Morales RY, Ortega Cisneros S, Camacho Perez JR, Sandoval Ibarra F, Casas Carrillo R. 3d simulation-based acoustic wave resonator analysis and validation using novel finite element method software. *Sensors.* 2021;21(8):2715.
70. Zhou Z, Xu Y, Qiao C, Liu L, Jia Y. A novel low-cost gas sensor for co2 detection using polymer-coated fiber Bragg grating. *Sens Actuators B Chem.* 2021;332: 129482.
71. Mirea T, Olivares J, Clement M, Iborra E. Impact of fbar design on its sensitivity as in-liquid gravimetric sensor. *Sens Actuators A.* 2019;289:87–93.
72. Mohammed HY, Farea MA, Ali ZM, Shirsat SM, Tsai M-L, Shirsat MD. Poly (n-methyl pyrrole) decorated rgo nanocomposite: A novel ultrasensitive and selective carbon monoxide sensor. *Chem Eng J.* 2022;441: 136010.
73. Shao S, Che L, Chen Y, Lai M, Huang S, Koehn R. A novel rgo-mos2-cds nanocomposite film for application in the ultrasensitive NO₂ detection. *J Alloy Compd.* 2019;774:1–10.
74. Dey A. Semiconductor metal oxide gas sensors: a review. *Mater Sci Eng B.* 2018;229:206–17.
75. Yang W, Gan L, Li H, Zhai T. Two-dimensional layered nanomaterials for gas-sensing applications. *Inorg Chem Front.* 2016;3(4):433–51.
76. Choi S-J, Kim I-D. Recent developments in 2d nanomaterials for chemiresistive-type gas sensors. *Electron Mater Lett.* 2018;14(3):221–60.
77. Sharma B, Kim J-S. Mems based highly sensitive dual fet gas sensor using graphene decorated pd-ag alloy nanoparticles for h2 detection. *Sci Rep.* 2018;8(1):1–9.
78. Qi P, Zhang T, Shao J, Yang B, Fei T, Wang R. A qcm humidity sensor constructed by graphene quantum dots and chitosan composites. *Sens Actuators A.* 2019;287:93–101.
79. Gao N, Li H-Y, Zhang W, Zhang Y, Zeng Y, Zhixiang H, Liu J, Jiang J, Miao L, Yi F, et al. Qcm-based humidity sensor and sensing properties employing colloidal SnO₂ nanowires. *Sens Actuators B Chem.* 2019;293:129–35.
80. Roto R, Rianjanu A, Fatyadi IA, Kusumaatmaja A, Triyana K. Enhanced sensitivity and selectivity of ammonia sensing by qcm modified with boric acid-doped pvac nanofiber. *Sens Actuators A.* 2020;304: 111902.
81. Hoang ND, Van Cat V, Nam MH, Phan VN, Le AT, Van Quy N. Enhanced so2 sensing characteristics of multi-wall carbon nanotubes based mass-type sensor using two-step purification process. *Sens Actuators A.* 2019;295:696–702.
82. Xu J, Bertke M, Li X, Mu H, Zhou H, Yu F, Hamdana G, Schmidt A, Bremers H, Peiner E. Fabrication of zno nanorods and chitosan@ zno nanorods on mems piezoresistive self-actuating silicon microcantilever for humidity sensing. *Sens Actuators B Chem.* 2018;273:276–87.
83. Li Z, Wang N, Lin Z, Wang J, Liu W, Sun K, Fu YQ, Wang Z. Room-temperature high-performance h2s sensor based on porous CuO nanosheets prepared by hydrothermal method. *ACS Appl Mater Interfaces.* 2016;8(32):20962–8.
84. Wang J, Zhou Q, Lu Z, Wei Z, Zeng W. The novel 2d honeycomb-like NiO nanoplates assembled by nanosheet arrays with excellent gas sensing performance. *Mater Lett.* 2019;255: 126523.
85. Guan Y, Wang D, Zhou X, Sun P, Wang H, Ma J, Lu G. Hydrothermal preparation and gas sensing properties of Zn-doped SnO₂ hierarchical architectures. *Sens Actuators B Chem.* 2014;191:45–52.
86. Wang Y, Yao L, Xu L, Wu W, Lin W, Zheng C, Feng Y, Gao X. One-step solvothermal synthesis of hierarchical wo3 hollow microspheres with excellent no gas sensing properties. *Mater Lett.* 2021;302: 130460.
87. Zhu J, Liu X, Shi Q, He T, Sun Z, Guo X, Liu W, Sulaiman OB, Dong B, Lee C. Development trends and perspectives of future sensors and mems/nems. *Micromachines.* 2019;11(1):7.
88. Zhao C, Gong H, Niu G, Wang F. Mems gas sensors-from nanomaterials to microelectrodes. In: 2020 IEEE 33rd International Conference on Micro Electro Mechanical Systems (MEMS), 2020;pp. 194–199. IEEE
89. Raninec M. Overcoming the technical challenges of electrochemical gas sensing, Technical Article. Norwood: MA, USA, Analog Devices 2019. p. 1–5.
90. Kim Y, Kang S-K, Oh N-C, Lee H-D, Lee S-M, Park J, Kim H. Improved sensitivity in Schottky contacted two-dimensional mos2 gas sensor. *ACS Appl Mater Interfaces.* 2019;11(42):38902–9.
91. Wusiman M, Taghipour F. Methods and mechanisms of gas sensor selectivity. *Crit Rev Solid State Mater Sci.* 2022;47(3):416–35.

92. Gao X, Zhang T. An overview: facet-dependent metal oxide semiconductor gas sensors. *Sens Actuators B Chem.* 2018;277:604–33.
93. Rzaiz JM, Nawaf SO, Ibrahim AK. A review on tin dioxide gas sensor: The role of the metal oxide doping, nanoparticles, and operating temperatures 2022.
94. Wang N, Tao W, Gong X, Zhao L, Wang T, Zhao L, Liu F, Liu X, Sun P, Lu G. Highly sensitive and selective NO₂ gas sensor fabricated from Cu₂O-cuO microflowers. *Sens Actuators B Chem.* 2022;362: 131803.
95. Zou C, Hu J, Su Y, Zhou Z, Cai B, Tao Z, Huo T, Hu N, Zhang Y. Highly repeatable and sensitive three-dimensional γ-Fe₂O₃@ reduced graphene oxide gas sensors by magnetic-field assisted assembly process. *Sens Actuators B Chem.* 2020;306:127546.
96. Zhang D, Zong X, Wu Z. Fabrication of tin disulfide/graphene oxide nanoflower on flexible substrate for ultrasensitive humidity sensing with ultralow hysteresis and good reversibility. *Sens Actuators B Chem.* 2019;287:398–407.
97. Liu X, Cheng S, Liu H, Hu S, Zhang D, Ning H. A survey on gas sensing technology. *Sensors.* 2012;12(7):9635–65.
98. Padvi M, Moholkar A, Prasad S, Prasad N. A critical review on design and development of gas sensing materials. *Eng Sci.* 2021;15:20–37.
99. Raghu AV, Karuppanan KK, Nampoothiri J, Pullithadathil B. Wearable, flexible ethanol gas sensor based on TiO₂ nanoparticles-grafted 2D-titanium carbide nanosheets. *ACS Appl Nano Mater.* 2019;2(3):1152–63.
100. Gruber B, David F, Sandra P. Capillary gas chromatography-mass spectrometry: current trends and perspectives. *TrAC, Trends Anal Chem.* 2020;124: 115475.
101. Zhou Z, Wang Z, Lin L. *Microsystems and nanotechnology.* New York: Springer; 2012.
102. Upadhyaya AM, Hasan MK, Abdel-Khalek S, Hassan R, Srivastava MC, Sharan P, Islam S, Saad AME, Vo N. A comprehensive review on the optical micro-electromechanical sensors for the biomedical application. *Frontiers in Public Health* 2021;9.
103. Bhugra H, Piazza G. *Piezoelectric MEMS Resonators.* New York: Springer; 2017.
104. Blachowicz T, Ehrmann A. 3d printed MEMS technology-recent developments and applications. *Micromachines.* 2020;11(4):434.
105. Rao KS, Sateesh J, Guha K, Baishnab K, Ashok P, Sravani KG. Design and analysis of MEMS based piezoelectric micro pump integrated with micro needle. *Microsyst Technol.* 2020;26(10):3153–9.
106. Qian J-Y, Hou C-W, Li X-J, Jin Z-J. Actuation mechanism of microvalves: a review. *Micromachines.* 2020;11(2):172.
107. Cugat O, Delamare J, Reyne G. Magnetic micro-actuators and systems (magmas). *IEEE Trans Magn.* 2003;39(6):3607–12.
108. Feng H, Miao X, Yang Z. Design, simulation and experimental study of the linear magnetic microactuator. *Micromachines.* 2018;9(9):454.
109. Rathod VT. A review of electric impedance matching techniques for piezoelectric sensors, actuators and transducers. *Electronics.* 2019;8(2):169.
110. Kus F, Altinkok C, Zayim E, Erdemir S, Tasaltin C, Guro I. Surface acoustic wave (SAW) sensor for volatile organic compounds (VOCs) detection with calix [4] arene functionalized gold nanorods (AUNRs) and silver nanocubes (AGNCs). *Sens Actuators B Chem.* 2021;330: 129402.
111. Mujahid A, Afzal A, Dickert FL. An overview of high frequency acoustic sensors-QCMs, SAWs and FBARs-chemical and biochemical applications. *Sensors.* 2019;19(20):4395.
112. Fu YQ, Luo J, Nguyen N-T, Walton A, Flewitt AJ, Zu X-T, Li Y, McHale G, Matthews A, Iborra E, et al. Advances in piezoelectric thin films for acoustic biosensors, acoustofluidics and lab-on-chip applications. *Prog Mater Sci.* 2017;89:31–91.
113. Kumar A, Prajesh R. The potential of acoustic wave devices for gas sensing applications. *Sensors Actuators A: Phys.* 2022. 113498.
114. Cheng CJ. Design, Modeling and Fabrication of Shear Mode Bulk Acoustic Wave Sensor as a Potential Biosensor, 2012.
115. Liu J, Chen D, Wang P, Song G, Zhang X, Li Z, Wang Y, Wang J, Yang J. A microfabricated thickness shear mode electroacoustic resonator for the label-free detection of cardiac troponin in serum. *Talanta.* 2020;215: 120890.
116. Wang L, Wang C, Wang Y, Quan A, Keshavarz M, Madeira BP, Zhang H, Wang C, Kraft M. A review on coupled bulk acoustic wave MEMS resonators. *Sensors.* 2022;22(10):3857.
117. Farget S, Hentz S, Puget P, Arcamone J, Matheron M, Colinet E, Andreucci P, Duraffourg L, Myers E, Roukes M. Gas sensors based on gravimetric detection—a review. *Sens Actuators B Chem.* 2011;160(1):804–21.
118. Bjurström J, Rosen D, Katardjiev I, Yanchev VM, Petrov I. Dependence of the electromechanical coupling on the degree of orientation of c-textured thin AlN films. *IEEE Trans Ultrason Ferroelectr Freq Control.* 2004;51(10):1347–53.
119. Pang W, Zhao H, Kim ES, Zhang H, Yu H, Hu X. Piezoelectric microelectromechanical resonant sensors for chemical and biological detection. *Lab Chip.* 2012;12(1):29–44.
120. Fogel R, et al. Bulk and surface acoustic wave sensor arrays for multi-analyte detection: a review. *Biosens Bioelectron.* 2019;163: 112164.
121. Mastromatteo U, Villa F. High sensitivity acoustic wave AlN/Si mass detectors arrays for artificial olfactory and biosensing applications: a review. *Sens Actuators B Chem.* 2013;179:319–27.
122. Toda K. Lamb-wave delay lines with interdigital electrodes. *J Appl Phys.* 1973;44(1):56–62.
123. Bjurström J, Katardjiev I, Yanchev V. Lateral-field-excited thin-film Lamb wave resonator. *Appl Phys Lett.* 2005;86(15): 154103.
124. Piazza G. Piezoelectric Aluminum Nitride Vibrating RF MEMS for Radio Front-end Technology, 2005.
125. Piazza G, Stephanou PJ, Pisano AP. Piezoelectric aluminum nitride vibrating contour-mode MEMS resonators. *J Microelectromech Syst.* 2006;15(6):1406–18.
126. Zou J. High-performance Aluminum Nitride Lamb Wave Resonators for RF Front-end Technology, 2015.
127. Hou Y, Zhang M, Han G, Si C, Zhao Y, Ning J. A review: aluminum nitride MEMS contour-mode resonator. *J Semicond.* 2016;37(10): 101001.
128. Jung SI, Ryu C, Piazza G, Kim HJ. A study on the effects of bottom electrode designs on aluminum nitride contour-mode resonators. *Micromachines.* 2019;10(11):758.
129. Fei S, Ren H. Temperature characteristics of a contour mode MEMS AlN piezoelectric ring resonator on SOI substrate. *Micromachines.* 2021;12(2):143.
130. Xu C, Kochhar A, Piazza G. Dynamic Q-enhancement in aluminum nitride contour-mode resonators. *Appl Phys Lett.* 2019;115(17): 173504.
131. Yanchev V, Katardjiev I. Thin film Lamb wave resonators in frequency control and sensing applications: a review. *J Micromech Microeng.* 2013;23(4): 043001.
132. Arapan L, Alexieva G, Avramov ID, Radeva E, Strashilov V, Katardjiev I, Yanchev V. Highly mass-sensitive thin film plate acoustic resonators (fpar). *Sensors.* 2011;11(7):6942–53.
133. Luo T, Liu W, Wen Z, Xie Y, Tong X, Cai Y, Liu Y, Sun C. A high-sensitivity gravimetric biosensor based on S₁ mode Lamb wave resonator. *Sensors.* 2022;22(15):5912.

134. Luo T, Liu Y, Zou Y, Zhou J, Liu W, Wu G, Cai Y, Sun C. Design and optimization of the dual-mode lamb wave resonator and dual-passband filter. *Micromachines*. 2022;13(1):87.
135. Shao S, Luo Z, Wu T. Optimization of s1 lamb wave resonators with a10. 8sc0. 2n. In: 2021 IEEE 16th International Conference on Nano/Micro Engineered and Molecular Systems (NEMS), 2021:p. 1523–1526. IEEE
136. Pang W, Zhang M, Liang J, Huang Q. Piezoelectric micro/nano mechanical devices for frequency control and chemical sensing. In: *Micro Electro Mechanical Systems. Micro/Nano Technologies vol. 2*. Springer, 2017.
137. Zhao Z, Qian Z, Wang B. Energy trapping of thickness-extensional modes in thin film bulk acoustic wave filters. *AIP Adv*. 2016;6(1):015002.
138. Zhang H, Pang W, Kim ES. Miniature high-frequency longitudinal wave mass sensors in liquid. *IEEE Trans Ultrason Ferroelectr Freq Control*. 2011;58(1):255–8.
139. Zhao H, Pang W, Zhang H. Piezoelectric acoustic resonant mass sensors. In: *Advances in Optoelectronics and Micro/nano-optics*, 2010:pp. 1–4. IEEE
140. Karabalin R, Matheny M, Feng X, Defaj E, Le Rhun G, Marcoux C, Hentz S, Andreucci P, Roukes M. Piezoelectric nanoelectromechanical resonators based on aluminum nitride thin films. *Appl Phys Lett*. 2009;95(10): 103111.
141. Thundat T, Wachter E, Sharp S, Warmack R. Detection of mercury vapor using resonating microcantilevers. *Appl Phys Lett*. 1995;66(13):1695–7.
142. Vashist SK. A review of microcantilevers for sensing applications. *J Nanotechnol*. 2007;3:1–18.
143. Pei J, Tian F, Thundat T. Glucose biosensor based on the microcantilever. *Anal Chem*. 2004;76(2):292–7.
144. Faegh S, Jalili N, Sridhar S. Ultrasensitive piezoelectric-based microcantilever biosensor: theory and experiment. *IEEE/ASME Trans Mecha-tron*. 2014;20(1):308–12.
145. Leahy S. *Developing Electrokinetic Cantilever Biosensors*, 2017.
146. Rugar D, Hansma P. Atomic force microscopy. *Phys Today*. 1990;43(10):23–30.
147. Binnig G, Quate C, Gerber C. Atomic force microscope. *physical review letters*. *Phys Rev Lett*. 1986;56(9).
148. Sepaniak M, Datskos P, Lavrik N, Tipple C. Peer reviewed: Microcantilever transducers: a new approach in sensor technology. *ACS Publica-tions*; 2002.
149. Waggoner PS, Craighead HG. Micro-and nanomechanical sensors for environmental, chemical, and biological detection. *Lab Chip*. 2007;7(10):1238–55.
150. Alvarez M, Lechuga LM. Microcantilever-based platforms as biosensing tools. *Analyst*. 2010;135(5):827–36.
151. Buchapudi KR, Huang X, Yang X, Ji H-F, Thundat T. Microcantilever biosensors for chemicals and bioorganisms. *Analyst*. 2011;136(8):1539–56.
152. Thundat T, Oden P, Warmack R. Microcantilever sensors. *Microscale Thermophys Eng*. 1997;1(3):185–99.
153. Mouro J, Pinto R, Paoletti P, Tiribilli B. Microcantilever: dynamical response for mass sensing and fluid characterization. *Sensors*. 2020;21(1):115.
154. Shahraki ZN, Ghaderi R. Vibration and sensitivity analysis of piezoelectric microcantilever as a self-sensing sensor. *Eur Phys J Appl Phys*. 2019;87(2):20401.
155. Ardali JR, Ghaderi R, Raeiszadeh F. Effect of microbeam geometry on the nano-mass sensor performance. *Mech Ind*. 2019;20(3):304.
156. Wilfonger R, Bardell P, Chhabra D. The resonistor: a frequency selective device utilizing the mechanical resonance of a silicon substrate. *IBM J Res Dev*. 1968;12(1):113–8.
157. Brand O, Pourkamali S. Electrothermal excitation of resonant mems. *Resonant MEMS: fundamentals, implementation and application*, 2015:173–201
158. Guo K, Jiang B, Liu B, Li X, Wu Y, Tian S, Gao Z, Zong L, Yao S, Zhao M, et al. Study on the progress of piezoelectric microcantilever beam micromass sensor. In: *IOP Conference Series: Earth and Environmental Science*, 2021;vol. 651:p. 022091. IOP Publishing
159. Itoh T, Suga T. Force sensing microcantilever using sputtered zinc oxide thin film. *Appl Phys Lett*. 1994;64(1):37–9.
160. Yuan Y, Shyong Chow K, Du H, Wang P, Zhang M, Yu S, Liu B. A zno thin-film driven microcantilever for nanoscale actuation and sensing. *Int J Smart Nano Mater*. 2013;4(2):128–41.
161. Vancura C, Rüegg M, Li Y, Hagleitner C, Hierlemann A. Magnetically actuated complementary metal oxide semiconductor resonant cantilever gas sensor systems. *Anal Chem*. 2005;77(9):2690–9.
162. Dong J, Ferreira PM. Electrostatically actuated cantilever with soi-mems parallel kinematic xy stage. *J Microelectromech Syst*. 2009;18(3):641–51.
163. Kolesar Jr ES. Electronic nerve agent detector. Google Patents. US Patent 4,549,427 1985.
164. Lang HP. Cantilever-based gas sensing. In: *Solid State Gas Sensing*, Springer 2009:pp. 1–24.
165. Littrell R, Grosh K. Modeling and characterization of cantilever-based mems piezoelectric sensors and actuators. *J Microelectromech Syst*. 2012;21(2):406–13.
166. Shin S, Song S, Lee Y, Lee N, Park J, Park H, Lee J. Fabrication and sensing behavior of piezoelectric microcantilever for nanobalance. *Jpn J Appl Phys*. 2003;42(9S):6139.
167. Shin S, Paik J-K, Lee N-E, Park J-S, Park H-D, Lee J. Gas sensor application of piezoelectric cantilever nanobalance; electrical signal read-out. *Ferroelectrics*. 2005;328(1):59–65.
168. Zhou J, Li P, Zhang S, Huang Y, Yang P, Bao M, Ruan G. Self-excited piezoelectric microcantilever for gas detection. *Microelectron Eng*. 2003;69(1):37–46.
169. Trajicheva A, Politakos N, Pérez BT, Joseph Y, Gilev JB, Tomovska R. Qcm nanocomposite gas sensors-expanding the application of water-borne polymer composites based on graphene nanoribbon. *Polymer*. 2021;213: 123335.
170. Jandas P, Prabakaran K, Luo J, MG DH. Effective utilization of quartz crystal microbalance as a tool for biosensing applications. *Sens Actuators A*. 2021;331: 113020.
171. Pohanka M. The piezoelectric biosensors: principles and applications. *Int J Electrochem Sci*. 2017;12:496–506.
172. Skládal P. Piezoelectric biosensors. *TrAC, Trends Anal Chem*. 2016;79:127–33.
173. Sauerbrey G. Use of quartz vibrator for weighting thin films on a microbalance. *Z Angew Phys*. 1959;155:206–12.

174. Magna G, Belugina R, Mandoj F, Catini A, Legin AV, Paolesse R, Di Natale C. Experimental determination of the mass sensitivity of quartz microbalances coated by an optical dye. *Sens Actuators B Chem.* 2020;320: 128373.
175. Alev O, Sarıca N, Özdemir O, Arslan LC, Büyükköse S, Öztürk ZZ. Cu-doped zno nanorods based qcm sensor for hazardous gases. *J Alloy Compd.* 2020;826: 154177.
176. Gupta M, Hawari HF, Kumar P, Burhanudin ZA, Tansu N. Functionalized reduced graphene oxide thin films for ultrahigh co₂ gas sensing performance at room temperature. *Nanomaterials.* 2021;11(3):623.
177. Chen W, Deng F, Xu M, Wang J, Wei Z, Wang Y. Go/cu₂o nanocomposite based qcm gas sensor for trimethylamine detection under low concentrations. *Sens Actuators B Chem.* 2018;273:498–504.
178. Fauzi F, Rianjanu A, Santoso I, Triyana K. Gas and humidity sensing with quartz crystal microbalance (qcm) coated with graphene-based materials—a mini review. *Sens Actuators A.* 2021;330: 112837.
179. Tchalala MR, Belmabkhout Y, Adil K, Chappanda KN, Cadiou A, Bhatt PM, Salama KN, Eddaoudi M. Concurrent sensing of co₂ and h₂o from air using ultramicroporous fluorinated metal-organic frameworks: effect of transduction mechanism on the sensing performance. *ACS Appl Mater Interfaces.* 2018;11(1):1706–12.
180. White RM, Voltmer FW. Direct piezoelectric coupling to surface elastic waves. *Appl Phys Lett.* 1965;7(12):314–6.
181. Go DB, Atashbar MZ, Ramshani Z, Chang H-C. Surface acoustic wave devices for chemical sensing and microfluidics: a review and perspective. *Anal Methods.* 2017;9(28):4112–34.
182. Delsing P, Cleland AN, Schuetz MJ, Knörzer J, Giedke G, Cirac JI, Srinivasan K, Wu M, Balram KC, Bäuerle C, et al. The 2019 surface acoustic waves roadmap. *J Phys D Appl Phys.* 2019;52(35): 353001.
183. Wohltjen H, Dessy R. Surface acoustic wave probe for chemical analysis. i. introduction and instrument description. *Anal Chem.* 1979;51(9):1458–64.
184. Länge K. Bulk and surface acoustic wave sensor arrays for multi-analyte detection: a review. *Sensors.* 2019;19(24):5382.
185. Mujahid A, Dickert FL. Surface acoustic wave (saw) for chemical sensing applications of recognition layers. *Sensors.* 2017;17(12):2716.
186. Palla-Papavlu A, Voicu SI, Dinescu M. Sensitive materials and coating technologies for surface acoustic wave sensors. *Chemosensors.* 2021;9(5):105.
187. Kryshtal R, Medved A. Surface acoustic waves in dynamic magnonic crystals for microwave signals processing. *Ultrasonics.* 2019;94:60–4.
188. Morgan DP. Surface-wave devices for signal processing. *Stud Electr Electron Eng.* 1985;19.
189. Hsu J-C, Chao C-L. Full-wave modeling of micro-acoustofluidic devices driven by standing surface acoustic waves for microparticle acoustophoresis. *J Appl Phys.* 2020;128(12): 124502.
190. Balysheva O. Saw filters for mobile communications: achievements and prospects. *Wave Electronics and its Application in Information and Telecommunication Systems (WECONF).* 2019;2019:1–4.
191. Ikata O, Miyashita T, Matsuda T, Nishihara T, Satoh Y. Development of low-loss band-pass filters using saw resonators for portable telephones. In: *IEEE 1992 Ultrasonics Symposium Proceedings, 1992*;pp. 111–115. IEEE
192. Malocha DC, Carmichael C, Smith MS, Weeks A. Thin film acoustoelectric ghz saw amplifier design. In: *2018 IEEE International Ultrasonics Symposium (IUS), 2018*;pp. 1–4. IEEE
193. Zhang Y, Cai Y, Zhou J, Xie Y, Xu Q, Zou Y, Guo S, Xu H, Sun C, Liu S. Surface acoustic wave-based ultraviolet photodetectors: a review. *Sci Bull.* 2020;65(7):587–600.
194. Pan Y, Molin Q, Guo T, Zhang L, Cao B, Yang J, Wang W, Xue X. Wireless passive surface acoustic wave (saw) technology in gas sensing. *Sensor Rev.* 2021.
195. Hotel O, Poli J-P, Mer-Calfati C, Scorsone E, Saada S. A review of algorithms for saw sensors e-nose based volatile compound identification. *Sens Actuators B Chem.* 2018;255:2472–82.
196. Hughes-Riley T, Dias T. Developing an acoustic sensing yarn for health surveillance in a military setting. *Sensors.* 2018;18(5):1590.
197. Abraham N, Krishnakumar RR, Unni C, Philip D. Simulation studies on the responses of zno-cuo/cnt nanocomposite based saw sensor to various volatile organic chemicals. *J Sci: Adv Mater Dev.* 2019;4(1):125–31.
198. Takai T, Iwamoto H, Takamine Y, Fuyutsume T, Nakao T, Hiramoto M, Toi T, Koshino M. Ihp saw technology and its application to microacoustic components. In: *2017 IEEE International Ultrasonics Symposium (IUS), 2017*;pp. 1–8. IEEE
199. Reindl L, Scholl G, Ostertag T, Scherr H, Wolff U, Schmidt F. Theory and application of passive saw radio transponders as sensors. *IEEE Trans Ultrason Ferroelectr Freq Control.* 1998;45(5):1281–92.
200. Hallil H, Dejous C, Hage-Ali S, Elmazria O, Rossignol J, Stuerger D, Talbi A, Mazzamurro A, Joubert P-Y, Lefeuvre E. Passive resonant sensors: trends and future prospects. *IEEE Sens J.* 2021;21(11):12618–32.
201. Ollé EP, Farré-Lladós J, Casals-Terré J. Advancements in microfabricated gas sensors and microanalytical tools for the sensitive and selective detection of odors. *Sensors.* 2020;20(19):5478.
202. Carmichael CP, Smith MS, Weeks AR, Malocha DC. Experimental investigation of surface acoustic wave acoustoelectric effect using a graphene film on lithium niobate. *IEEE Trans Ultrason Ferroelectr Freq Control.* 2018;65(11):2205–7.
203. Laidoudi F, Boubenider F, Caliendo C, Hamidullah M. Numerical investigation of rayleigh, sezawa and love modes in c-axis tilted zno/si for gas and liquid multimode sensor. *J Mech.* 2020;36(1):7–18.
204. Zou J, Lin C-M, Lam C, Pisano AP. Transducer design for aln lamb wave resonators. *J Appl Phys.* 2017;121(15): 154502.
205. Jiang C, Chen Y, Cho C. A three-dimensional finite element analysis model for sh-saw torque sensors. *Sensors.* 2019;19(19):4290.
206. Rayleigh L. On waves propagated along the plane surface of an elastic solid. *Proc Lond Math Soc.* 1885;1(1):4–11.
207. Fu C, Ke Y, Quan A, Li C, Fan X, Ou J, Luo J. Investigation of Rayleigh wave and love wave modes in 112 0 zno film based multilayer structure. *Surf Coat Technol.* 2019;363:330–7.
208. Su Y, Li C, Li M, Li H, Xu S, Qian L, Yang B. Surface acoustic wave humidity sensor based on three-dimensional architecture graphene/pva/sio₂ and its application for respiration monitoring. *Sens Actuators B Chem.* 2020;308: 127693.
209. Ballantine D Jr, White RM, Martin SJ, Ricco AJ, Zellers E, Frye G, Wohltjen H. *Acoustic wave sensors: theory design and physico-chemical Applications.* Amsterdam: Elsevier; 1996.
210. Moutoulas E, Hamidullah M, Prodromakis T. Surface acoustic wave resonators for wireless sensor network applications in the 433.92 mhz ism band. *Sensors.* 2020;20(15):4294.

211. Auld BA. *Acoustic Fields and Waves in Solids*. Ripol Classic Publishing House; 1973.
212. Wohltjen H. Mechanism of operation and design considerations for surface acoustic wave device vapour sensors. *Sensors Actuators*. 1984;5(4):307–25.
213. Liu J, Lu Y. Response mechanism for surface acoustic wave gas sensors based on surface-adsorption. *Sensors*. 2014;14(4):6844–53.
214. Djoumi L, Vanotti M, Blondeau-Patissier V. Real time cascade impactor based on surface acoustic wave delay lines for pm10 and pm2. 5 mass concentration measurement. *Sensors*. 2018;18(1):255.
215. Devkota J, Kim K-J, Ohodnicki PR, Culp JT, Greve DW, Lekse JW. Zeolitic imidazolate framework-coated acoustic sensors for room temperature detection of carbon dioxide and methane. *Nanoscale*. 2018;10(17):8075–87.
216. Devkota J, Greve DW, Hong T, Kim K-J, Ohodnicki PR. An 860 mhz wireless surface acoustic wave sensor with a metal-organic framework sensing layer for co 2 and ch 4. *IEEE Sens J*. 2020;20(17):9740–7.
217. Li M, Kan H, Chen S, Feng X, Li H, Li C, Fu C, Quan A, Sun H, Luo J, et al. Colloidal quantum dot-based surface acoustic wave sensors for NO₂-sensing behavior. *Sens Actuators B Chem*. 2019;287:241–9.
218. Tang Y, Ao D, Li W, Zu X, Li S, Fu YQ. NH₃ sensing property and mechanisms of quartz surface acoustic wave sensors deposited with sio₂, tio₂, and sio₂-tio₂ composite films. *Sens Actuators B Chem*. 2018;254:1165–73.
219. Smyth KM. Piezoelectric micro-machined ultrasonic transducers for medical imaging. PhD thesis, Massachusetts Institute of Technology 2017.
220. Smyth K, Sodini C, Kim SG. High electromechanical coupling piezoelectric micro-machined ultrasonic transducer (pmut) elements for medical imaging. In: 2017 19th International Conference on Solid-State Sensors, Actuators and Microsystems (TRANSDUCERS), 2017;pp. 966–969. IEEE
221. Balasingam JA. Design and modeling of piezoelectric micromachined ultrasonic transducer (pmut) using a multi-user mems process for medical imaging. PhD thesis, University of Windsor (Canada) 2020.
222. Jung J, Lee W, Kang W, Shin E, Ryu J, Choi H. Review of piezoelectric micromachined ultrasonic transducers and their applications. *J Micromech Microeng*. 2017;27(11): 113001.
223. Jiang X, Tang H-Y, Lu Y, Ng EJ, Tsai JM, Boser BE, Horsley DA. Ultrasonic fingerprint sensor with transmit beamforming based on a pmut array bonded to cmos circuitry. *IEEE Trans Ultrason Ferroelectr Freq Control*. 2017;64(9):1401–8.
224. Jiang X, Tang HY, Lu Y, Li X, Tsai JM, Ng EJ, Daneman MJ, Lim M, Assaderaghi F, Boser BE, et al. Monolithic 591×438 dpi ultrasonic fingerprint sensor. In: 2016 IEEE 29th International Conference on Micro Electro Mechanical Systems (MEMS), 2016;pp. 107–110. IEEE
225. Tang H-Y, Lu Y, Jiang X, Ng EJ, Tsai JM, Horsley DA, Boser BE. 3-d ultrasonic fingerprint sensor-on-a-chip. *IEEE J Solid-State Circuits*. 2016;51(11):2522–33.
226. Roy K, Gupta H, Shastri V, Dangi A, Jeyaseelan A, Dutta S, Pratap R. Fluid density sensing using piezoelectric micromachined ultrasound transducers. *IEEE Sens J*. 2019;20(13):6802–9.
227. Nazemi H, Antony Balasingam J, Swaminathan S, Ambrose K, Nathani MU, Ahmadi T, Babu Lopez Y, Emadi A. Mass sensors based on capacitive and piezoelectric micromachined ultrasonic transducers-cmut and pmut. *Sensors*. 2020;20(7):2010.
228. Sun C, Jiang S, Liu Y. Numerical study and optimisation of a novel single-element dual-frequency ultrasound transducer. *Sensors*. 2018;18(3):703.
229. Sun C, Shi Q, Yazici MS, Lee C, Liu Y. Development of a highly sensitive humidity sensor based on a piezoelectric micromachined ultrasonic transducer array functionalized with graphene oxide thin film. *Sensors*. 2018;18(12):4352.
230. Qiu Y, Gigliotti JV, Wallace M, Griggio F, Demore CE, Cochran S, Trolier-McKinstry S. Piezoelectric micromachined ultrasound transducer (pmut) arrays for integrated sensing, actuation and imaging. *Sensors*. 2015;15(4):8020–41.
231. Shirakawa A, Pham JM, Jarry P, Kerhervé E. Design of fbar filters at high frequency bands. *International Journal of RF and Microwave Computer-Aided Engineering: Co-sponsored by the Center for Advanced Manufacturing and Packaging of Microwave, Optical, and Digital Electronics (CAMPmode) at the University of Colorado at Boulder*. 2007;17(1):115–22.
232. Ruby RC, Bradley P, Oshmyansky Y, Chien A, Larson JD. Thin film bulk wave acoustic resonators (fbar) for wireless applications. In: 2001 IEEE Ultrasonics Symposium. Proceedings. An International Symposium (Cat. No. 01CH37263), 2001;vol. 1;pp. 813–821. IEEE
233. Koohi MZ, Mortazawi A. Negative piezoelectric-based electric-field-actuated mode-switchable multilayer ferroelectric fbars for selective control of harmonic resonances without degrading k². *IEEE Trans Ultrason Ferroelectr Freq Control*. 2020;67(9):1922–30.
234. Yandrapalli S, Liffredo M, Faizan M, Küçük S, Maillard D, Villanueva LG. Thin film devices for 5g communications. In: 2021 IEEE 34th International Conference on Micro Electro Mechanical Systems (MEMS), 2021;pp. 450–453. IEEE
235. Aigner R, Fattinger G. 3g–4g–5g: How baw filter technology enables a connected world. In: 2019 20th International Conference on Solid-State Sensors, Actuators and Microsystems & Eurosensors XXXIII (TRANSDUCERS & EUROSENSORS XXXIII), 2019;pp. 523–526. IEEE
236. Ruppel CC. Acoustic wave filter technology-a review. *IEEE Trans Ultrason Ferroelectr Freq Control*. 2017;64(9):1390–400.
237. Bradley P, Lee S, Kang M, Kim J. Fbar duplexers with minimal shunt inductance for better isolation and packing density. In: 2019 IEEE International Ultrasonics Symposium (IUS), 2019;pp. 1693–1695. IEEE
238. Hagelauer A, Fattinger G, Ruppel CC, Ueda M, Hashimoto K-Y, Tag A. Microwave acoustic wave devices: Recent advances on architectures, modeling, materials, and packaging. *IEEE Trans Microw Theory Tech*. 2018;66(10):4548–62.
239. Ruby R, Bradley P, Clark D, Feld D, Jamneala T, Wang K. Acoustic fbar for filters, duplexers and front end modules. In: 2004 IEEE MTT-S International Microwave Symposium Digest (IEEE Cat. No. 04CH37535), 2004;vol. 2;pp. 931–934. IEEE
240. Zhang H, Dong S, Chen W, Han Y. Mimo multiplexer based on film bulk acoustic resonator. *IEEE Trans Consum Electron*. 2010;56(2):805–10.
241. Snyder RV, Mortazawi A, Hunter I, Bastioli S, Macchiarella G, Wu K. Present and future trends in filters and multiplexers. *IEEE Trans Microw Theory Tech*. 2015;63(10):3324–60.
242. Hu J, Qu H, Guo W, Chang Y, Pang W, Duan X. Film bulk acoustic wave resonator for trace chemical warfare agents simulants detection in micro chromatography. In: 2019 20th International Conference on Solid-State Sensors, Actuators and Microsystems & Eurosensors XXXIII (TRANSDUCERS & EUROSENSORS XXXIII), 2019;pp. 45–48. IEEE
243. Gabl R, Green E, Schreiter M, Feucht H, Zeininger H, Primig R, Pitzer D, Eckstein G, Wersing W. Novel integrated fbar sensors: a universal technology platform for bio-and gas-detection. In: *SENSORS, 2003 IEEE, 2003;vol. 2;pp. 1184–1188. IEEE*

244. Hashwan SSB, Khir MM, Al-Douri Y, Algamili AS, Alabsi SS. Design and simulation of ain-based fbar resonator for hydrogen sulfide gas detection. In: 2021 IEEE International Conference on Sensors and Nanotechnology (SENNANO), 2021;pp. 73–76. IEEE
245. Hashwan SSB, Khir MM, Al-Douri Y, Ahmed AY, Algamili AS, Alabsi SS, Junaid MM. Analytical modeling of ain-based film bulk acoustic wave resonator for hydrogen sulfide gas detection based on piezomumps. In: Journal of Physics: Conference Series, 2021;vol. 1962;p. 012003. IOP Publishing
246. Rughoobur G, DeMiguel-Ramos M, Escolano JM, Iborra E, Flewitt AJ. Gravimetric sensors operating on inclined c-axis zno grown at 1.1 ghz based on textured al electrodes. *Sci Rep.* 2017;7(1):1–9.
247. Hashwan SSB, Khir MHB, Al-Douri Y, Ahmed AY. Recent progress in the development of biosensors for chemicals and pesticides detection. *IEEE Access.* 2020;8:82514–27.
248. Lakin K, Wang J. Acoustic bulk wave composite resonators. *Appl Phys Lett.* 1981;38(3):125–7.
249. Grudkowski T, Black J, Reeder T, Cullen D, Wagner R. Fundamental-mode vhf/uhf minature acoustic resonators and filters on silicon. *Appl Phys Lett.* 1980;37(11):993–5.
250. Nakamura K, Sasaki H, Shimizu H. A piezoelectric composite resonator consisting of a zno film on an anisotropically etched silicon substrate. *Jpn J Appl Phys.* 1981;20(S3):111.
251. Sliker T, Roberts D. A thin-film cds-quartz composite resonator. *J Appl Phys.* 1967;38(5):2350–8.
252. Coussot G. Bulk wave resonator for the 100-300 mhz frequency range. In: 1974 Ultrasonics Symposium, 1974;pp. 590–591. IEEE
253. Roberts D, Koneval D, Sliker T. Alternate approaches to high frequency filter crystals. In: 21st Annual Symposium on Frequency Control, 1967;pp. 83–114. IEEE
254. Thompson M, Kipling AL, Duncan-Hewitt WC, Rajaković LV, Čavić-Vlasak BA. Thickness-shear-mode acoustic wave sensors in the liquid phase. a review. *Analyst.* 1991;116(9):881–90.
255. Benetti M, Cannata D, D'Amico A, Di Pietrantonio F, Foglietti V, Verona E. Thin film bulk acoustic wave resonator (tfbar) gas sensor. In: IEEE Ultrasonics Symposium, 2004, 2004;vol. 3;pp. 1581–1584. IEEE
256. Artieda A, Muralt P. High-q aln/sio₂ symmetric composite thin film bulk acoustic wave resonators. *IEEE Trans Ultrason Ferroelectr Freq Control.* 2008;55(11):2463–8.
257. Zhang Y, Luo J, Flewitt AJ, Cai Z, Zhao X. Film bulk acoustic resonators (fbars) as biosensors: A review. *Biosens Bioelectron.* 2018;116:1–15.
258. Johar AK, Sharma GK, Periasamy C, Guha K, Agarwal A, Boolchandani D. Investigating the effect of various bragg's reflector configurations on the performance of flexible fbar sensors. In: *Micro and Nanoelectronics Devices, Circuits and Systems, 2022*;pp. 129–138. Springer.
259. Qi B, Lu Y, Hua D, Cai C. Resonate frequency research on material characteristics of fbar temperature sensor. In: 2017 IEEE 9th International Conference on Communication Software and Networks (ICCSN), 2017;pp. 344–348. IEEE
260. Ren J, Chu H, Bai Y, Wang R, Chen P, Chen J. Research and design of high sensitivity fbar micro-mass sensors. In: *IOP Conference Series: Earth and Environmental Science, 2021*;vol. 632;p. 042014. IOP Publishing
261. Xue Y, Zhou C, Zhang XY, Chan M. A flexible high quality-factor bulk acoustic resonator enabled with transferred single-crystal piezoelectric thin film for sensing applications. *Sens Actuators, A.* 2021;326: 112721.
262. Ndoye M, Kerroum I, Deslandes D, Domingue F. Air-filled substrate integrated cavity resonator for humidity sensing. *Sens Actuators B Chem.* 2017;252:951–5.
263. Wang X, Liang J-G, Wu J-K, Gu X-F, Kim N-Y. Microwave detection with various sensitive materials for humidity sensing. *Sens Actuators B Chem.* 2022;351: 130935.
264. Huang S, Luo W, Bai X, Lv L, Pan X, Shuai Y, Wu C, Zhang W. A solidly mounted resonator fabricated by linbo 3 single-crystalline film on flexible polyimide substrate. *IEEE Trans Ultrason Ferroelectr Freq Control.* 2021;68(7):2585–9.
265. Kim H-Y, Kim K-B, Cho SH, Kim Y-I. Analysis of resonance characteristics of bragg reflector type film bulk acoustic resonator. *Surf Coat Technol.* 2012;211:143–7.
266. Johar AK, Varma T, Periasamy C, Agarwal A, Boolchandani D. Design, analysis and finite element modeling of solidly mounted film bulk acoustic resonator for gas sensing applications. *J Electron Mater.* 2020;49(2):1503–11.
267. Choi N, Kim K, Kim Y, Kim M. Effect of design parameters on thin film bulk acoustic resonator performance. *J Electroceram.* 2014;33(1):17–24.
268. Gao C, Jiang Y, Zhang L, Liu B, Zhang M. An investigation on efficient acoustic energy reflection of flexible film bulk acoustic resonators. *Nanotechnology and Precision Engineering.* 2018;1(2):129–32.
269. Yang T, Chen W, Wang P. A review of all-optical photoacoustic spectroscopy as a gas sensing method. *Appl Spectrosc Rev.* 2021;56(2):143–70.
270. Jiang Y, Zhang M, Duan X, Zhang H, Pang W. A flexible, gigahertz, and free-standing thin film piezoelectric mems resonator with high figure of merit. *Appl Phys Lett.* 2017;111(2): 023505.
271. Lu Y, Zhang M, Zhang H, Jiang Y, Zhang H, Pang W. Microfluidic bulk-modulus measurement by a nanowavelength longitudinal-acoustic-wave microsensors in the nonreflective regime. *Phys Rev Appl.* 2019;11(4): 044091.
272. Yanez J, Uranga A, Barniol N. Multi-frequency thin film hbar microsensors for acoustic impedance sensing over the ghz range. In: 2021 21st International Conference on Solid-State Sensors, Actuators and Microsystems (Transducers), 2021;pp. 1347–1350. IEEE
273. Veselov A, Elmanov V, Kiryasova O, Nikulin YV. Damping of longitudinal and shear acoustic waves in a structure with zno films with straight and inclined textures. *Tech Phys.* 2017;62(3):470–4.
274. Chen Y-C, Shih W-C, Chang W-T, Yang C-H, Kao K-S, Cheng C-C. Biosensor for human ige detection using shear-mode fbar devices. *Nanoscale Res Lett.* 2015;10(1):1–8.
275. Chen YC, Chang WT, Kao KS, Yang CH, Cheng CC. The liquid sensor using thin film bulk acoustic resonator with c-axis tilted aln films. *Journal of Nanomaterials* 2013;**2013**.
276. Fu Y-Q, Pang H-F, Torun H, Tao R, McHale G, Reboud J, Tao K, Zhou J, Luo J, Gibson D, et al. Engineering inclined orientations of piezoelectric films for integrated acoustofluidics and lab-on-a-chip operated in liquid environments. *Lab Chip.* 2021;21(2):254–71.
277. Qin L, Chen Q, Cheng H, Wang Q-M. Analytical study of dual-mode thin film bulk acoustic resonators (fbars) based on zno and aln films with tilted c-axis orientation. *IEEE Trans Ultrason Ferroelectr Freq Control.* 2010;57(8):1840–53.

278. Liu W, Qu H, Hu J, Pang W, Zhang H, Duan X. A highly sensitive humidity sensor based on ultrahigh-frequency microelectromechanical resonator coated with nano-assembled polyelectrolyte thin films. *Micromachines*. 2017;8(4):116.
279. Hu J, Qu H, Chang Y, Pang W, Zhang Q, Liu J, Duan X. Miniaturized polymer coated film bulk acoustic wave resonator sensor array for quantitative gas chromatographic analysis. *Sens Actuators B Chem*. 2018;274:419–26.
280. Liu J, Zhao Z, Fang Z, Liu Z, Zhu Y, Du L. High-performance fbar humidity sensor based on the pi film as the multifunctional layer. *Sens Actuators B Chem*. 2020;308: 127694.
281. Liu J, Workie TB, Wu T, Wu Z, Gong K, Bao J, Hashimoto Ky. Q-factor enhancement of thin-film piezoelectric-on-silicon mems resonator by phononic crystal-reflector composite structure. *Micromachines*. 2020;11(12):1130.
282. Workie TB, Liu J, Wu Z, Tang P, Bao JF, Hashimoto Ky. Swastika hole shaped phononic crystal for quality enhancement of contour mode resonators. In: 2021 IEEE MTT-S International Wireless Symposium (IWS), 2021:pp. 1–3. IEEE
283. Zou J, Lin CM, Pisano AP. Anchor loss suppression using butterfly-shaped plates for aln lamb wave resonators. In: 2015 Joint Conference of the IEEE International Frequency Control Symposium & the European Frequency and Time Forum, 2015:pp. 432–435. IEEE
284. Segovia-Fernandez J, Cremonesi M, Cassella C, Frangi A, Piazza G. Anchor losses in aln contour mode resonators. *J Microelectromech Syst*. 2014;24(2):265–75.
285. Zhou X, Liu J, Bao F, Song Y, Bao J, Zhang X. Fish scale-shaped acoustic reflector array for quality factor enhancement of aln-on-silicon mems resonator. In: 2019 IEEE International Ultrasonics Symposium (IUS), 2019:pp. 1720–1723. IEEE
286. Bao F-H, Bao L-L, Zhang X-S, Zhang C, Li X-Y, Qin F, Zhang T, Zhang Y, Wu Z-H, Bao J-F. Frame structure for thin-film piezoelectric-on-silicon resonator to greatly enhance quality factor and suppress spurious modes. *Sens Actuators, A*. 2018;274:101–8.
287. Kumar Y, Rangra K, Agarwal R. Design and simulation of fbar for quality factor enhancement. *Mapan*. 2017;32(2):113–9.
288. Guo H, Gao Y, Liu T. A theoretical study of the voc sensor based on polymer-coated diaphragm embedded with fbar. *Measurement*. 2018;129:206–10.
289. Rathod VT. A review of acoustic impedance matching techniques for piezoelectric sensors and transducers. *Sensors*. 2020;20(14):4051.
290. Pons-Nin J, Gorreta S, Domínguez M, Blokhina E, O'Connell D, Feely O. Design and test of resonators using piezomumps technology. In: 2014 Symposium on Design, Test, Integration and Packaging of MEMS/MOEMS (DTIP), 2014:pp. 1–6. IEEE
291. Cowen A, Hames G, Glukh K, Hardy B. Piezomumps design handbook. MEMSCAP Inc 2014;1.
292. Zaszczynska A, Grady A, Sajkiewicz P. Progress in the applications of smart piezoelectric materials for medical devices. *Polymers*. 2020;12(11):2754.
293. Chen C, Wang X, Wang Y, Yang D, Yao F, Zhang W, Wang B, Sewvandi GA, Yang D, Hu D. Additive manufacturing of piezoelectric materials. *Adv Func Mater*. 2020;30(52):2005141.
294. Fawzy A, Zhang M. Piezoelectric thin film materials for acoustic mems devices. In: 2019 6th International Conference on Advanced Control Circuits and Systems (ACCS) & 2019 5th International Conference on New Paradigms in Electronics & Information Technology (PEIT), 2019:pp. 82–86. IEEE
295. García-Gancedo L, Zhu Z, Iborra E, Clement M, Olivares J, Flewitt A, Milne W, Ashley G, Luo J, Zhao X, et al. Aln-based baw resonators with cnt electrodes for gravimetric biosensing. *Sens Actuators B Chem*. 2011;160(1):1386–93.
296. Chang Y, Tang N, Qu H, Liu J, Zhang D, Zhang H, Pang W, Duan X. Detection of volatile organic compounds by self-assembled monolayer coated sensor array with concentration-independent fingerprints. *Sci Rep*. 2016;6(1):1–12.
297. Chen D, Yang L, Yu W, Wu M, Wang W, Wang H. Micro-electromechanical acoustic resonator coated with polyethyleneimine nanofibers for the detection of formaldehyde vapor. *Micromachines*. 2018;9(2):62.
298. Wang W, Chen D, Wang H, Yu W, Wu M, Yang L. Film bulk acoustic formaldehyde sensor with layer-by-layer assembled carbon nanotubes/polyethyleneimine multilayers. *J Phys D Appl Phys*. 2018;51(5): 055104.
299. Wang J, Zhan D, Wang K, Hang W. The detection of formaldehyde using microelectromechanical acoustic resonator with multiwalled carbon nanotubes-polyethyleneimine composite coating. *J Micromech Microeng*. 2017;28(1): 015003.
300. Song S, Chen D, Wang H, Guo Q, Wang W, Wu M, Yu W. Film bulk acoustic formaldehyde sensor with polyethyleneimine-modified single-wall carbon nanotubes as sensitive layer. *Sens Actuators B Chem*. 2018;266:204–12.
301. Ma J, Wang S, Chen D, Wang W, Zhang Z, Song S, Yu W. Zn piezoelectric film resonator modified with multi-walled carbon nanotubes/polyethyleneimine bilayer for the detection of trace formaldehyde. *Appl Phys A*. 2018;124(1):1–9.
302. Zeng G, Wu C, Chang Y, Zhou C, Chen B, Zhang M, Li J, Duan X, Yang Q, Pang W. Detection and discrimination of volatile organic compounds using a single film bulk acoustic wave resonator with temperature modulation as a multiparameter virtual sensor array. *ACS sensors*. 2019;4(6):1524–33.
303. Yan X, Qu H, Chang Y, Pang W, Wang Y, Duan X. Surface engineering of metal-organic framework prepared on film bulk acoustic resonator for vapor detection. *ACS applied materials & interfaces*. 2020;12(8):10009–17.
304. Hui Z, Yan X, Qu H, Pang W, Duan X. Zeolitic imidazolate framework modified film bulk acoustic resonator for highly sensitive and selective alcohol vapors detection. In: 2019 20th International Conference on Solid-State Sensors, Actuators and Microsystems & Eurosensors XXXIII (TRANSDUCERS & EUROSensors XXXIII), 2019:pp. 1325–1328. IEEE
305. Zhang M, Du L, Fang Z, Zhao Z. A sensitivity-enhanced film bulk acoustic resonator gas sensor with an oscillator circuit and its detection application. *Micromachines*. 2017;8(1):25.
306. Hoffmann R, Schreiter M, Heitmann J. The concept of thin film bulk acoustic resonators as selective co₂ gas sensors. *Journal of Sensors and Sensor Systems*. 2017;6(1):87–96.
307. Choi S, Drese JH, Jones CW. Adsorbent materials for carbon dioxide capture from large anthropogenic point sources. *ChemSusChem: Chemistry & Sustainability Energy & Materials*. 2009;2(9):796–854.
308. Yu C-H, Huang C-H, Tan C-S, et al. A review of co₂ capture by absorption and adsorption. *Aerosol and Air Quality Research*. 2012;12(5):745–69.
309. Kumar S, Srivastava R, Koh J. Utilization of zeolites as co₂ capturing agents: Advances and future perspectives. *J CO₂ Util*. 2020;41:101251.
310. Trickett CA, Helal A, Al-Maythalony BA, Yamani ZH, Cordova KE, Yaghi OM. The chemistry of metal-organic frameworks for co₂ capture, regeneration and conversion. *Nat Rev Mater*. 2017;2(8):1–16.
311. D'Alessandro DM, Smit B, Long JR. Carbon dioxide capture: prospects for new materials. *Angew Chem Int Ed*. 2010;49(35):6058–82.

312. Yu KMK, Curcic I, Gabriel J, Tsang SCE. Recent advances in CO₂ capture and utilization. *ChemSusChem: Chemistry & Sustainability Energy & Materials*. 2008;1(11):893–9.
313. Xu X, Wang J, Long Y. Zeolite-based materials for gas sensors. *Sensors*. 2006;6(12):1751–64.
314. Ashraf N, Mesbah Y, Emad A, Mostafa H. Enabling the 5G: Modelling and design of high Q film bulk acoustic wave resonator (fbar) for high frequency applications. In: 2020 IEEE International Symposium on Circuits and Systems (ISCAS), 2020;pp. 1–4. IEEE
315. Jiang P, Mao S, An Z, Fei C, Lou L, Li Z, Zhao T, Jiang S, Yang Y. Structure-size optimization and fabrication of 3.7 GHz film bulk acoustic resonator based on AlN thin film. *Frontiers in Materials*, 2021:343.
316. Duan FL, Yang Z, Ji Z, Weng H, Xie Z, Shen A, Mi S, Chen X, Chen Y, Liu Q. Process optimization and device variation of Mg-doped ZnO fbars. *Solid-State Electron*. 2019;151:11–7.
317. Fang Z, Jin H, Dong S, Lu L, Xuan W, Luo J. Ultrathin single-crystalline LiNbO₃ film bulk acoustic resonator for 5G communication. *Electron Lett*. 2020;56(21):1142–3.
318. Song Y, Perez C, Esteves G, Lundh JS, Saltonstall CB, Beechem TE, Yang JI, Ferri K, Brown JE, Tang Z, et al. Thermal conductivity of aluminum scandium nitride for 5G mobile applications and beyond. *ACS Applied Materials & Interfaces*. 2021;13(16):19031–41.
319. Yanez J, Ledesma E, Uranga A, Barniol N. AlN-based hbar ultrasonic sensor for fluid detection in microchannels with multi-frequency operation capability over the GHz range. In: 2021 IEEE International Ultrasonics Symposium (IUS), 2021;pp. 1–4. IEEE
320. Yanez J, Uranga A, Barniol N. Fluid compressional properties sensing at microscale using a longitudinal bulk acoustic wave transducer operated in a pulse-echo scheme. *Sens Actuators, A*. 2022;334: 113334.
321. Zhang J, Zhang X, Wei X, Xue Y, Wan H, Wang P. Recent advances in acoustic wave biosensors for the detection of disease-related biomarkers: A review. *Anal Chim Acta*. 2021;1164: 338321.
322. Terzieva M, Gaydazhiev D, Nikolova B. 2d multiphysics frequency simulations of thin-film bulk acoustic wave resonator. In: 2017 40th International Spring Seminar on Electronics Technology (ISSE), 2017;pp. 1–5. IEEE
323. Liu J, Du J, Wang J, Yang J. Thin film bulk acoustic wave piezoelectric resonators with circular ring driving electrodes for mass sensing. *Integr Ferroelectr*. 2018;192(1):57–66.
324. Sabani Z, Ralib AAM, Karim J, Saidin NB, Razali NFBM. Design and simulation of film bulk acoustic wave resonator (fbar) gas sensor based on ZnO thin film. In: 2019 IEEE Regional Symposium on Micro and Nanoelectronics (RSM), 2019;pp. 34–37. IEEE
325. Mohd Nor NI, Shah K, Singh J, Sauli Z. Design and simulation of film bulk acoustic wave resonator in Ku-band. In: *Advanced Materials Research*, 2013;vol. 662;pp. 556–561. Trans Tech Publ
326. Zhang T, Liang F, Li M, Li S, Pang H, Wang S, Zhu H, Yan Z, Zhao S. Theoretical simulation and optimization on material parameters of thin film bulk acoustic resonator. *Journal of Nanomaterials* 2015;2015.
327. Johar AK, Sharma GK, Kumar TB, Varma T, Periasamy C, Agarwal A, Boolchandani D. Optimization of a flexible film bulk acoustic resonator-based toluene gas sensor. *J Electron Mater*. 2021;50(9):5387–95.
328. Balasubramani V, Chandraleka S, Rao TS, Sasikumar R, Kuppusamy M, Sridhar T. Recent advances in electrochemical impedance spectroscopy based toxic gas sensors using semiconducting metal oxides. *J Electrochem Soc*. 2020;167: 037572.
329. Popa D, Udrea F. Towards integrated mid-infrared gas sensors. *Sensors*. 2019;19:2076.
330. Park NH, Akamatsu T, Itoh T, Izu N, Shin W. Calorimetric thermoelectric gas sensor for the detection of hydrogen, methane and mixed gases. *Sensors*. 2014;14:8350–62.
331. Feng L, Feng L, Li Q, Cui J, Guo J. Sensitive formaldehyde detection with QCM sensor based on PAAm/MWCNTs and PVAm/MWCNTs. *ACS Omega*. 2021;6:14004–14.
332. Yang M, He J. Graphene oxide as quartz crystal microbalance sensing layers for detection of formaldehyde. *Sens Actuators B Chem*. 2016;228:486–90.
333. Sarango L, Benito J, Gascon I, Zornoza B, Coronas J. Homogeneous thin coatings of zeolitic imidazolate frameworks prepared on quartz crystal sensors for CO₂ adsorption. *Microporous Mesoporous Mater*. 2018;272:44–52.
334. Tai H, Bao X, He Y, Du X, Xie G, Jiang Y. Enhanced formaldehyde-sensing performances of mixed polyethyleneimine-multiwalled carbon nanotubes composite films on quartz crystal microbalance. *IEEE Sens J*. 2015;15:6904–11.
335. Kang Z, Zhang D, Li T, Liu X, Song X. Polydopamine-modified SnO₂ nanofiber composite coated QCM gas sensor for high-performance formaldehyde sensing. *Sens Actuators B Chem*. 2021;345: 130299.
336. Xu S, Li C, Li H, Li M, Qu C, Yang B. Carbon dioxide sensors based on a surface acoustic wave device with a graphene-nickel-L-alanine multilayer film. *Journal of Materials Chemistry C*. 2015;3:3882–90.
337. Xu S, Zhang R, Cui J, Liu T, Sui X, Han M, Zheng F, Hu X. Surface Acoustic Wave DMMP Gas Sensor with a Porous Graphene/PVDF Molecularly Imprinted Sensing Membrane. *Micromachines*. 2021;12:552.
338. Tang Q, Guo Y, Tang YL, Long G, Wang J, Li D, Zu XT, Ma J, Wang L, Torun H, et al. Highly sensitive and selective Love mode surface acoustic wave ammonia sensor based on graphene oxides operated at room temperature. *J Mater Sci*. 2019;54:11925–35.
339. Luo J, Feng X, Kan H, Li H, Fu C. One-Dimensional Bi₂S₃ Nanobelts-Based Surface Acoustic Wave Sensor for NO₂ Detection at Room Temperature. *IEEE Sens J*. 2020;21:1404–8.
340. Tang Y, Xu X, Han S, Cai C, Du H, Zhu H, Zu X, Fu Y. ZnO-Al₂O₃ nanocomposite as a sensitive layer for high performance surface acoustic wave H₂S gas sensor with enhanced elastic loading effect. *Sens Actuators B Chem*. 2020;304: 127395.
341. Xu X, Zu X, Ao D, Yu J, Xiang X, Xie W, Tang Y, Li S, Fu Y. NH₃-sensing mechanism using surface acoustic wave sensor with AlO(OH) film. *Nanomaterials*. 2019;9:1732.
342. Tang Y, Wu W, Wang B, Dai X, Xie W, Yang Y, Zhang R, Shi X, Zhu H, Luo J, et al. H₂S gas sensing performance and mechanisms using CuO-Al₂O₃ composite films based on both surface acoustic wave and chemiresistor techniques. *Sens Actuators B Chem*. 2020;325: 128742.
343. Zhu H, Xie D, Lin S, Zhang W, Yang Y, Zhang R, Shi X, Wang H, Zhang Z, Zu X, et al. Elastic loading enhanced NH₃ sensing for surface acoustic wave sensor with highly porous nitrogen doped diamond like carbon film. *Sens Actuators B Chem*. 2021;344: 130175.
344. Rana L, Gupta R, Tomar M, Gupta V. ZnO/ST-Quartz SAW resonator: An efficient NO₂ gas sensor. *Sens Actuators B Chem*. 2017;252:840–5.
345. Li D, Zu X, Ao D, Tang Q, Fu Y, Guo Y, Bilawal K, Faheem MB, Li L, Li S, et al. High humidity enhanced surface acoustic wave (SAW) H₂S sensors based on sol-gel CuO films. *Sens Actuators B Chem*. 2019;294:55–61.
346. Boyadjiev SI, Rassovska MM. WO₃ thin films deposition on quartz crystal resonators for applications in gas sensors. *Electronics* 2007;2007.

347. Debeda H, Dufour I. Resonant microcantilever devices for gas sensing. In: *Advanced nanomaterials for inexpensive gas microsensors*. Elsevier; 2020. p. 161–88.
348. DeMiguel-Ramos M, Diaz-Duran B, Escolano JM, Barba M, Mirea T, Olivares J, Clement M, Iborra E. Gravimetric biosensor based on a 1.3 GHz AlN shear-mode solidly mounted resonator. *Sens Actuators B Chem*. 2017;239:1282–8.
349. Kozlov A, Torgash T. Analytical study of microelectronic piezoelectric resonators based on bulk acoustic waves with an aluminum-aluminum oxide film electrode. In: *Proceedings of the 2022 Wave Electronics and its Application in Information and Telecommunication Systems (WECONF)*. IEEE; 2022. p. 1–5.
350. Patel R, Bansal D, Agrawal VK, Rangra K, Boolchandani D. Fabrication and RF characterization of zinc oxide based film bulk acoustic resonator. *Superlattices Microstruct*. 2018;118:104–15.
351. Lee TY, Song JT. Detection of carcinoembryonic antigen using AlN FBAR. *Thin Solid Films*. 2010;518:6630–3.

Publisher's Note Springer Nature remains neutral with regard to jurisdictional claims in published maps and institutional affiliations.